Spring 6-13-2014

Experimental Investigation of Lateral Cyclic Behavior of Wood-Based Screen-Grid Insulated Concrete Form Walls

John Stuart Garth
Portland State University

Experimental Investigation of Lateral Cyclic Behavior of Wood-Based Screen-Grid Insulated Concrete Form Walls

by

John Stuart Garth

A thesis submitted in partial fulfillment of the
requirements for the degree of

Master of Science
in
Civil and Environmental Engineering

Thesis Committee:
Peter Dusicka, Chair
Corey Griffin
Franz Rad

Portland State University
2014

ABSTRACT

Insulated concrete forms (ICFs) are green building components that are primarily used for residential wall construction. Unlike most polystyrene based ICF variants, the Faswall ICFs used in these experiments were significantly denser because they were made from recycled wood particles and cement. The current design approach for structures constructed with this type of wall form only allows the designer to consider the contribution of the reinforced concrete cores. Previous research has shown that this approach may be conservative. This project experimentally evaluated the lateral structural response of these types of grid ICF walls under increasing amplitude of in-plane cyclic loading. Two different height-to-length (aspect) ratios (approximately 2:1 and 1:1) were investigated, as was the effect of simultaneous gravity load. Furthermore, the reinforced concrete grid was exposed for each aspect ratio in order to examine the contribution of the ICF blocks to the lateral response. Analyses of hysteretic behaviors and failure modes indicated conservatism in the current design approach for estimating lateral strength and ignoring the beneficial contribution of the ICF blocks to overall performance. The presence of the wall forms increased the lateral shear capacity of the walls by an average of 42% (compared to the walls with forms removed), while also increasing the deformation capacity by an average of 102%. Furthermore, by considering an additional gravity load of 10 kips-per-lineal-foot (klf), the shear resistance of the walls increased by 32% (versus walls only subjected to self-weight), on average, and the deformation capacity of the walls increased by an average of 19%. Comparisons of the

experimental results to several design equations led to the recommendation of a design equation that was previously accepted for another type of ICF system.

ACKNOWLEDGEMENTS

I would first like to acknowledge my advisor and committee chair, Dr. Peter Dusicka. I am grateful for the opportunities you have given me in the lab, as well as the knowledge and experience that I have obtained while working with you.

I would also like to acknowledge Dr. Franz Rad and Mr. Corey Griffin for their questions and suggestions which helped improve this thesis.

Thank you to OregonBest for the grants that made this research possible. Thank you to Shelterworks, Ltd. for providing the ICFs used in this project.

Thanks to my colleagues in iSTAR (past and present) for their assistance, especially with placing concrete. Thank you specifically to Arlindo Lopes, Marshall Stokes, and Max Stephens for all of your advice and support.

Finally, thank you to my family. Thank you to my parents – your love, guidance, and support has not only shaped who I am but also contributed greatly to any success I have had. Thank you to my brother and sister-in-law. It's been a great comfort having you guys in Portland and I appreciate you keeping me fed.

TABLE OF CONTENTS

LIST OF TABLES

LIST OF FIGURES

Chapter 1: INTRODUCTION

Insulated concrete forms (ICFs) are green building components that are primarily used in residential construction. Although there are several types of ICFs (e.g., screen-grid, waffle-grid, and flat), the principles behind each remain the same. ICFs are stay-in-place forms that have reinforced concrete cores. The presence of the ICF wall forms reduces the amount of concrete, relative to a purely reinforced concrete system, required to complete a job. Buildings constructed with ICFs can be very energy efficient due to the high R-value and thermal mass of the blocks. Figure 1-1 shows the three types of ICF walls mentioned above.

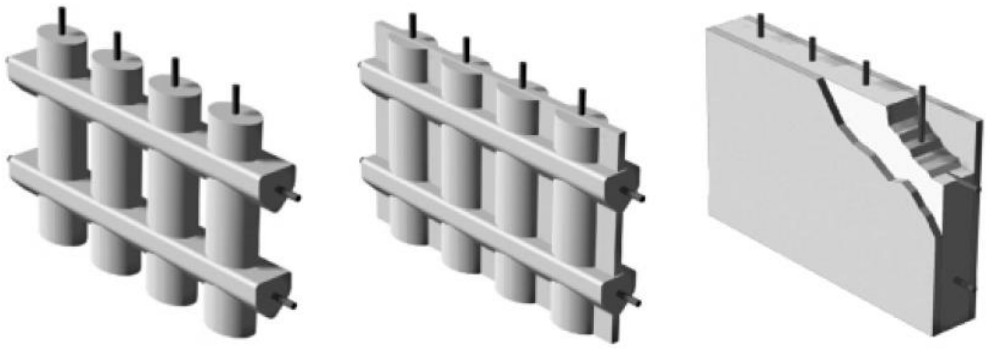

Figure 1-1: Types of ICFs. From left to right: screen-grid (with forms removed), waffle grid (with forms removed), and flat. Images from PCA (2003).

Screen-grid ICFs (SGICFs) differ from the other two wall form types in that they are the only ICF type that has spaces, which are occupied by the wall form material, between the reinforced concrete cores. This creates reinforced concrete matrix consisting of horizontal and vertical cores. Waffle-grid ICFs are similar in this manner, but these forms are constructed in such a way that allows the cores to be connected by thinner

(relative to the cores) concrete plates. Flat ICF walls consist of two wall forms that sandwich what amounts to a typical reinforced concrete wall.

There are several types of materials used to create ICFs. Two of the more common materials are expanded polystyrene (EPS) foam and recycled wood chips, both of which are bonded with cement. The wall forms featured in this procedure are constructed with the latter material type.

1.1. **Background**

The wall forms that were used in this study were Faswall ICFs, which were supplied by ShelterWorks, LTD. The composition of these forms is 85% mineralized wood chips and 15% cement. The mineralization of the wood chips is a proprietary process that results in a product that is able to resist rot and mold. In addition to these attributes, walls constructed from these forms have a four hour fire rating, are termite resistant, require little to no bracing during placement of concrete, and have performance R values between 30 and 35.

Each Faswall form has an insulating sleeve as well as horizontal and vertical cutouts that create, when stacked, internal grids that are filled with concrete and reinforcing steel. Walls built using these forms, then, are screen-grid ICF walls. More details about the Faswall wall forms and the internal grid layout are discussed in Section 2.1, which discusses wall construction.

1.2. **Literature Review**

The papers and studies included in this section were the ones deemed most germane and comparable to the objectives and results of this procedure.

1.2.1. Full-Scale Tests at Portland State University

This testing sequence yielded both a paper (Dusicka et al. 2011) and a report (Kay et al. 2008). Overall, this investigation examined 13 screen-grid ICF specimens and six reinforced concrete shear walls, which were designed using an equivalent thickness of the circular ICF concrete cores. The ICF specimens were 128-in-tall expanded polystyrene (EPS) screen-grid (APEX) ICF walls with two different aspect (height-to-length) ratios (0.89:1 and 2.67:1). For each aspect ratio, six walls were tested: three under self-weight and three under an added axial load of 10 klf. The other ICF specimen was a wall with the lower aspect ratio in which the ICFs had been stripped so that only the reinforced concrete cores remained. This specimen was not subjected to any additional axial load. Three reinforced concrete walls were tested at each aspect ratio, but none of these walls were subjected to additional gravity loading. The displacement controlled cyclic loading protocol was developed in accordance with ACI T1.101 (2001) and ACI ITG-5.1 (2008), as prescribed by Hawkins et al. (2004), and was the same loading protocol used for this procedure.

As stated above, the APEX ICF blocks were formed using EPS concrete. The blocks were 10 in wide, 16 in tall, and 48 in long. Both the horizontal and vertical cores had 6 in diameters and were spaced 16 in on center. One straight #4 reinforcing bar was used per core. In order to mimic standard construction practice, no rebar was tied. For the

dowels, or starter bars, #5 reinforcing steel was used for each vertical core. The dowels stuck out 30 in above the foundation block in order to conform to ACI 318 standards for lap splices. All reinforcing steel was Grade 60. The 0.89:1 aspect ratio walls also had a six-inch wide by four-inch deep bond beam to better facilitate the transfer of load. The reinforced concrete shear walls had reinforcement at roughly the same spacing as the ICF walls and were 4.5 in thick in order to act as benchmarks to compare to the ICF walls in terms of in-plane shear capacity. The thickness of the walls was determined by taking the equivalent width of an ICF wall's cores to be 0.75 times the diameter of the cores.

The ICF walls with higher aspect ratios demonstrated flexural-controlled deformation behavior under loading. After failure, the ICFs were stripped from the walls in the failure zone in order to examine the cracking pattern. Walls under both types of gravity loading (self-weight and 10 klf) had the most damage occur in the extreme, or exterior, vertical cores. For the walls under self-weight only, the outer vertical cores showed flexural (horizontal) cracks, while the inner vertical cores had shear (diagonal) cracks. The walls with the additional 10 klf gravity load had minimal damage in their interior vertical cores and neither group had much damage in their horizontal cores.

The ICF walls with the lower aspect ratio had horizontal failure zones in which the outer vertical cores incurred the most damage, the interior vertical cores underwent severe shear cracking, and the horizontal cores were mostly unscathed. The walls that were subjected to only self-weight consistently had failure zones along the terminus of the lap-splice. Two of the walls that were subjected to the additional 10 klf gravity load

had failure zones 16 in below the bond beam, while the other wall's failure zone was the same as the self-weight group.

Results indicate that despite the low compressive strength of the ICF material (see Sections 1.2.2 and 1.2.3), the stay-in-place forms contribute significantly to a wall's lateral load resistance, drift capacity, stiffness, and ductility. The specimen that was tested without the ICFs showed, on average, a 17% reduction in ultimate strength, a 4% decrease in drift capacity, and a 45% reduction in the ductility ratio when compared to the walls that were tested with their forms still in place. The experiments also showed that the introduction of additional vertical load increased the lateral load resistance capabilities of the walls, but affected the walls' drift capacity differently depending on aspect ratio. For the higher aspect ratio walls, the introduction of the additional axial load resulted in a 57% increase in peak lateral load resistance but a 25% reduction of drift capacity. For the lower aspect ratio walls, the addition of the 10 klf axial load resulted in an average peak load increase of 27% and increase in drift capacity of 39%. The equivalent reinforced concrete walls had significantly higher peak loads than the ICF walls – the concrete walls with the 2.67:1 aspect ratio demonstrated shear resistance that was 53% greater than their ICF counterparts, while the walls with 0.89:1 aspect ratios resisted 82% more load than the ICF walls, on average.

1.2.2. Component Tests at Portland State University

This study, which was the thesis of Werner (2010), performed tests at a component level for two different ICF systems – APEX and Faswall – and also attempted to model each wall form type. Material tests were also performed on each type of form,

both to aid the modeling process and to show the performance of each wall form material at target strains. The components were tested with and without forms, with varying types of reinforcement, and different types of concrete. The tests showed that the ICFs contributed significantly to both the lateral strength and deformation capacity – increases of up to 100% and 60%, respectively – of the specimens. The models overestimated the lateral load resistance of the specimens by 50-100% and were completely unreliable in determining the drift capacity.

The APEX samples, which used the same type of ICFs used in Dusicka's and Kay's research, were 32 in tall and 35.5 in long. Because of these dimensions, there were three cores that ran parallel to the line of loading: one at the center, which was where the point of loading occurred, and two on either end. The two end cores were clamped to the load frame to act as supports. These specimens also had to have 1.25 in removed from their outer portions in order to fit into the load frame. With this specimen configuration, there were also two cores that were perpendicular to the line of action, which represented the vertical cores. The paper written by Dusicka et al. showed that the majority of the damage in the APEX walls occurred in the vertical cores. For Werner's procedures, the changes in reinforcement type were only made in the vertical cores.

The Faswall specimens were built and loaded in the same manner as the APEX sample; however, because of the block geometry, the specimens were 24"x32". These samples had three horizontal cores running parallel to the line of action, with one in the center at the point of loading, and two vertical cores perpendicular to the point of loading.

As was the case with the APEX samples, the reinforcement was only altered in the vertical cores of the Faswall specimens.

The modes of failure began the same way for each type of specimen. Flexural cracks would develop at the joints of the horizontal and vertical cores and these cracks would subsequently propagate to such a degree that the joints would act as hinges, where – at least for a large portion of each later cycle – the only resistance to load was from the reinforcement. A result of this was a significant reduction of the residual stiffness of the samples in later cycles, which could be seen as pinching in the hysteresis curves. After hinging occurred in the joints, typical modes of failure were due to severe diagonal shear cracks in the vertical cores or axial cracks in the plane of the reinforcement perpendicular to the direction of loading. A majority of the tests on Faswall specimens had to be cancelled before failure occurred due to damage in the horizontal support cores. The relative stiffness of the vertical cores to the horizontal cores was much higher for Faswall specimens than for the APEX specimens.

For the Faswall specimens with forms left in place, the maximum load resistance was at least 45% higher than the corresponding specimens with forms removed; however, the specimens with no forms in place had higher drift capacities. Similarly, the APEX specimens with the forms left in place demonstrated a 25% higher, on average, peak load resistance compared to the analogous specimens which had their forms stripped. Using fiber-reinforced (ECC) concrete instead of portland cement concrete (both were designed for a compressive strength of 4000 psi, but ended up being about 7000 psi) had little effect on load resistance, but significantly improved the deformation capacities of both

types of specimens. The fiber-reinforced mix used 8mm-long polyvinyl alcohol fibers at 2% of the volume of the mix. No coarse aggregate was used for this mix. The ECC concrete also showed peak strains between 0.3 and 0.4% in compression tests.

In addition to the component tests discussed above, Werner also conducted material tests on the different wall forms. Compression tests were performed on 6-in-long blocks of the Faswall material with 2-in by 2-in cross-sections. The results showed that, at 0.3% strain (the maximum strain expected in the concrete), the stress in the wood-based ICF material was between 20 and 70 psi, or about 0.3 to 1% of the actual stress that would be seen in the concrete (assuming a compressive strength of 7000 psi, as was demonstrated by both mixes used for the Faswall specimens) at that strain. The compression tests on the EPS concrete (from the APEX forms) were performed on cylinders that had 3.75-in diameters and were 7 in tall. These samples resisted between five and 20 psi at a strain of 0.3%.

1.2.3. Full-Scale and Material Tests from University of California, Irvine

This dissertation (Yland 2000) observed the behavior of twelve EPS screen-grid ICF walls subjected to in-plane cyclic loading, three walls under flexural monotonic loading, and two walls under eccentric axial loading and out-of-plane flexural loading. In addition to the wall tests, material tests were performed on the ICF wall material and concrete, both independently and as a composite material.

Two types of walls underwent displacement controlled in-plane cyclic loading. The first wall type (henceforth referred to as the standard wall type) was 10 ft tall and was representative of typical construction practices. Two aspect ratios, 1:1 and 2:1, were

used for this wall type. The other wall type was only a single block long and had three different aspect ratios: 3:1, 2.5:1, and 2:1. The ICFs used in this procedure were 10 in thick, 15 in tall, and 30 in long with 6-in diameter vertical and horizontal cores spaced 15 in on center. The mix design for each wall was 3000 psi and each wall was cast in a single lift with no vibration. For the standard walls, with the exception of a one preliminary 1:1 wall, which was intended to demonstrate the upper-bound of the walls' performance, the horizontal rebar was allowed to rest at the bottom of each core and the vertical rebar was hand-centered on the day of casting. None of the reinforcement was tied. The displacement controlled loading protocol consisted of three cycles per displacement and an increase in the target displacement for each subsequent set of cycles, much like the procedure used by PSU. Each wall was also subjected to an axial load of 10 klf.

Failure in the walls occurred at about 1% drift, though the walls with higher aspect ratios performed slightly better than those with lower aspect ratios. Though the average deformation capacity of the walls tested by Yland was noticeably lower than the APEX walls tested at PSU, the modes of failure were similar for the two wall types, i.e., horizontal cracking at or around the lap splice. The reduced deformation capacity (relative to the APEX walls) could be explained by differences in concrete strength, core geometry, and loading protocol. The concrete strength for the walls used in Yland's tests was around 3000 psi, while the strength of concrete used for the APEX tests at PSU was between about 4000-5000 psi. While the cores were the same size for each set of walls, the core spacing was 15 in on center for the walls tested by Yland and 16 in on center for

the APEX walls. The loading protocol utilized by Yland took 57 total cycles before reaching a target drift of 1%. The protocol used at PSU took 25 total cycles to reach the same target drift demand. The higher number of lower level cycles could have contributed to significant and premature degradation of the walls tested by Yland.

In addition to the wall tests, this procedure also considered the material properties of the EPS concrete used to form the ICFs as well as the properties of a batch of concrete that was allowed to cure under different circumstances. Compression tests were performed on 2”x2”x4” EPS concrete blocks and these tests showed that the blocks were able to withstand up to 50% strain, though their maximum strength was about 110 psi. But this peak strength occurred at a strain of about 12.5%, which was still considerably higher than the 0.3% ultimate strain expected for concrete. Tests were also performed to determine the Poisson’s ratio and the Young’s modulus for the EPS concrete in order to plug these values into a finite element model. The concrete tests (outside of the typical 7-day, 28-day, and day-of-testing cylinders) consisted of testing 2-in diameter by 4-in tall cylinders that had been cured in a mold, cast in a mold and then removed after several days to air dry, and cured in-situ. The cylinders that were cured in-situ were cast into 2-in diameter by 4-in tall cylindrical holes that had been bored into 6”x6”x4” EPS concrete blocks. The concrete mix used was designed to have 28-day strength of 3000 psi. These cylinders were tested with and without the forms in place. The 28-day results showed there was little difference between the air-dried and mold-cured cylinders (1800 psi and 1870 psi, respectively), but there was a 29% increase in compressive strength for the cylinders that had been cast in-situ and then stripped as compared to those that had been

mold-cured. The cylinders that were kept in the EPS concrete blocks during testing had a compressive strength that was 98% greater than the mold-cured cylinders. So, while the EPS concrete offered little resistance relative to the concrete at 0.3% strain, there was evidence to suggest that the low-density ICF material had a confining effect upon the concrete, which could partially explain the noticeable increase in lateral load resistance and deformation capabilities of the APEX walls tested at PSU with forms in place versus those whose forms had been stripped.

1.2.4. National Association of Home Builders Report

This study (NAHB 2001) examined the behavior of three types of ICF walls (flat, waffle-grid, and screen-grid) under in-plane shear loading. Height-to-length ratio, window and door openings, and minimal reinforcement details were all considered for their influence on the shear resistance capability of each type of ICF wall. The walls were subjected to pseudo-static monotonic loading as prescribed by (or similar to the prescriptions of) ASTM E72. Three screen-grid walls were tested for this procedure: one 4-ft long by 8-ft tall (2:1 aspect ratio) wall, one wall that was 12-ft by 8-ft with a 4-ft-long segment connected to a 2-ft-long segment by two 1-ft-tall lintels, top and bottom (creating a 6-ft by 6-ft lintel), and one wall that was 12-ft by 8-ft with a 7-ft by 8-ft opening in the center (creating two two-foot-long walls connected by an 8-ft by 1-ft lintel at the top) to mimic a garage door opening.

The screen-grid wall with no openings failed at 17.2 kips and about 1.8% drift from diagonal shear cracks and horizontal cracks in the vertical cores that were propagated from the point of load application. The window specimen failed at 5.6 kips

and 0.77% drift due to diagonal shear cracks in the four-foot wall segment. The screen-grid specimen with the garage opening was not tested past 1.6 kips at 1.2% drift because the specimen exhibited racking behavior. Major flexural cracking had already occurred in the corners of the opening.

Two models were used to predict the lateral load resistance of the walls. The first model assumed all wall segments together as a continuous wall to resist shear. The second model assumed each 4-ft segment was controlled by shear and that each 2-ft segment was controlled by flexure. Therefore, the models were identical for the walls with no openings and were based on ACI 318's prescriptions for shear capacity. This report only considered the contribution of the reinforced concrete cores to the shear capacity of the walls. These methods proved to be conservative for the screen-grid wall with no openings (42% less than the experimentally determined value) and non-conservative for the wall types with window (147% higher, on average, than the experimentally derived value) and door (273% higher, on average) openings, even though the second wall type may have failed prematurely.

1.3. **Research Objectives**

Since no full-scale in-plane shear tests had been conducted on an ICF wall constructed with the Faswall wall forms, the purpose of this study was to observe the performance of such a wall under a fully-reversed cyclic loading protocol. This loading protocol was developed to be representative of the loading sequence a structure might be subjected to in a seismic event. Performance was based on the lateral load resisting

capacity, drift capacity, modes of failure, ductility, energy dissipation, and residual stiffness of each specimen.

Current design standards dictate that, for any walls constructed with these wall forms, only the reinforced concrete cores can be considered to resist the expected in-plane lateral forces that would result from seismic loading. Given this practice, one objective of this experimental program was to quantify the contribution of the wall forms to the overall performance of the wall. In order to achieve this goal, certain walls had their wall forms removed after concrete had been placed and had been given reasonable time to cure. Previous testing (Werner 2009, Dusicka et al. 2011) has shown that ICFs can make a significant contribution to the overall performance of an SGICF wall.

This procedure also investigated how wall performance was affected by the addition of a distributed axial load that would be representative of the gravity loading a first story wall would experience in a three-story structure. The testing conducted by Dusicka et al (2011) showed that the addition of gravity loading to a shear wall can increase that wall's shear-resisting capabilities, which suggests that performing cyclic tests on walls without such loading can yield conservative results.

In addition to the results obtained from the testing executed in this study, the performance of these walls was compared to the performance of ICF walls, ICF components, and reinforced concrete shear walls that had been tested previously. Several theoretical measures of performance, which were based on existing codes as well as Faswall-specific load tables, were also considered and compared to the results of the Faswall wall tests.

The final objective, after conducting all of the testing and comparing all of the data, was to recommend a metric for future design of Faswall ICF walls. As mentioned before, the status quo of Faswall ICF wall design was to neglect the contribution of the ICFs, which, given the results from previous testing, may have been a conservative assumption. The existing load tables for simplified design of Faswall ICF shear walls also tended toward the conservative side, based on the results yielded from previous ICF tests.

Chapter 2: TEST SETUP

Many different components went into a single test. This section breaks down the entire test setup process, from construction of the wall specimens to completion of the testing sequences.

2.1. **Wall Construction**

The standard Faswall block was 8 in tall, 24 in long, and 12 in wide. The core dimensions are shown in Figure 2-1. Four types of end blocks were used in the construction of these walls: two that were 12 in long and two that were 24 in long. The difference between the blocks with same lengths was the finger-jointing patterns, which were referred to as male or female, depending on configuration. Figure 2-2 shows the different types of Faswall blocks currently used. The different end blocks made it so contiguous layers of blocks were staggered, which was consistent with standard construction practices. The first course (base level) of blocks was placed so that the bond beam notches were on top – as is shown in Figure 2-1. For the next course, the blocks were rotated 90 degrees so that the notches faced downwards. In this way, the channels for the horizontal cores were formed.

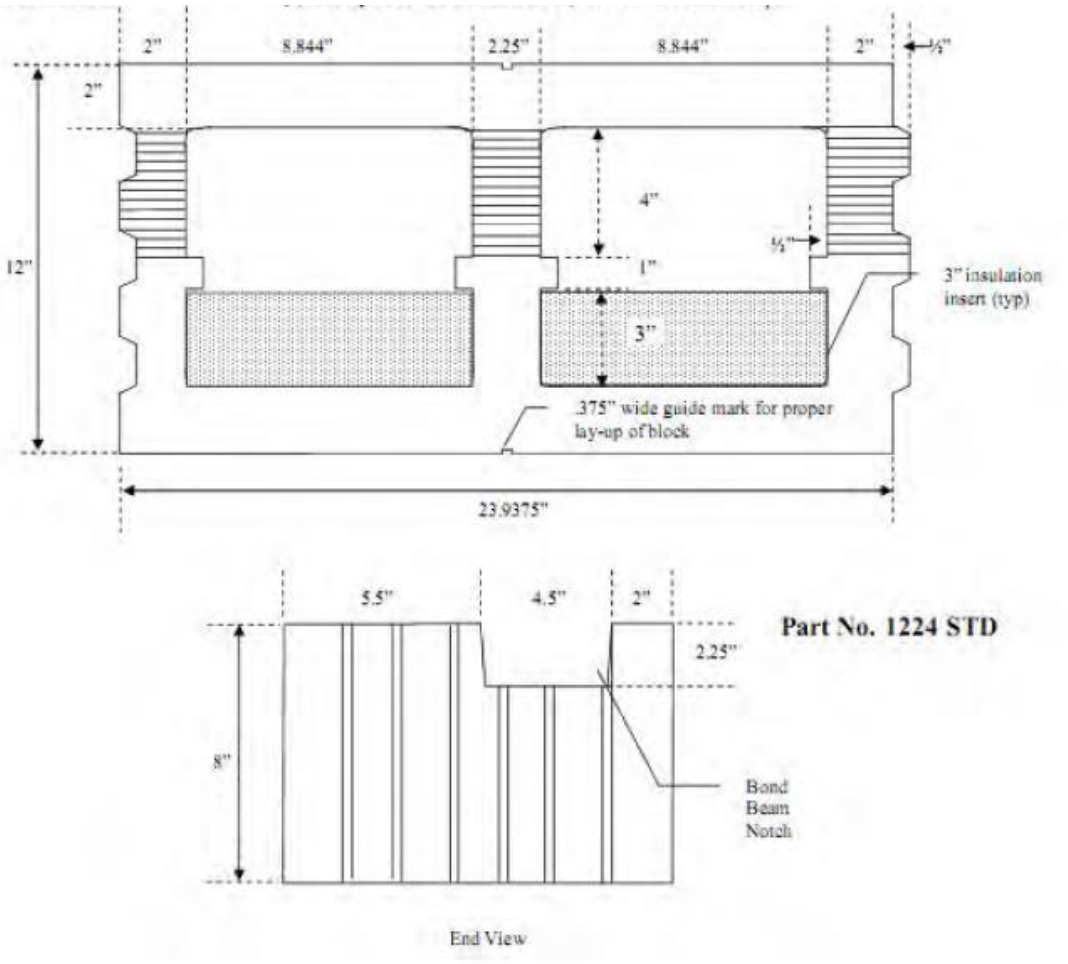

Figure 2-1: Standard Faswall wall form detail. Image from ShelterWorks, LTD (2010).

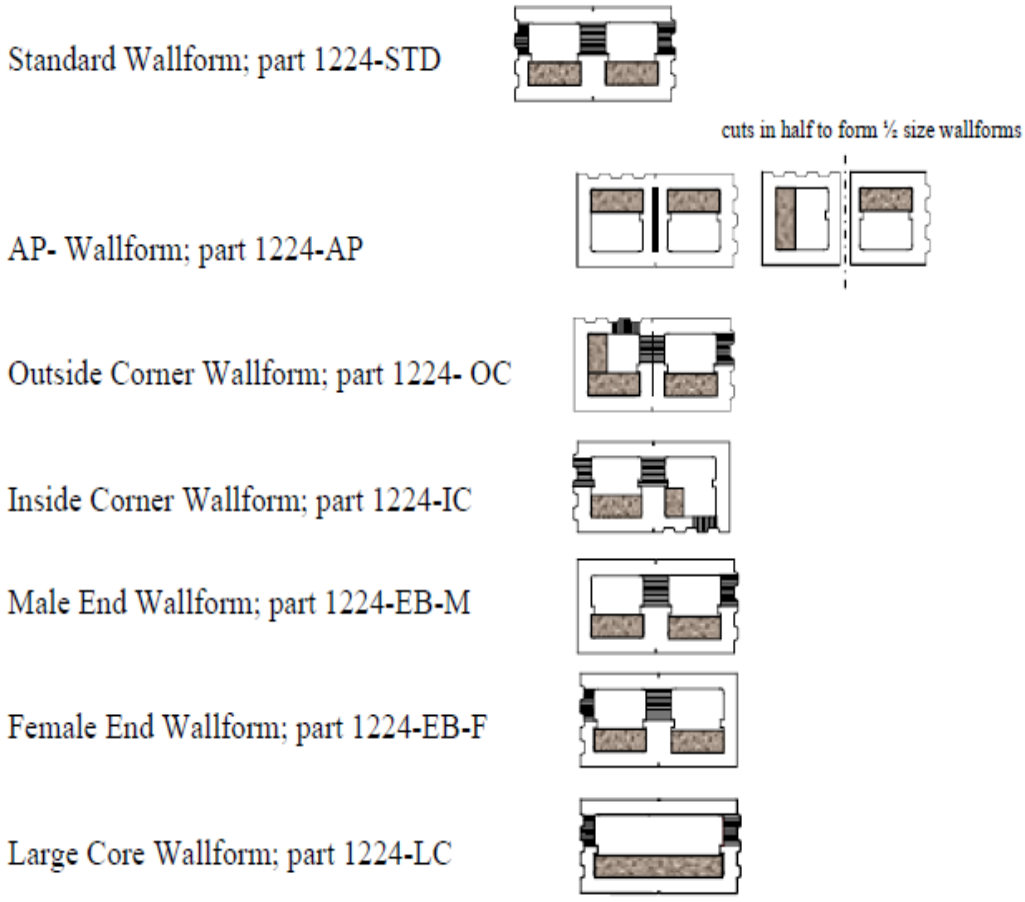

Figure 2-2: Faswall block configurations. Image from ShelterWorks, LTD (2010).

The baseline walls that were tested in this procedure had reinforcing in each core. The dowels used in each vertical core were Grade 60, #5 bars that stuck out 30 in above the foundation block in order to conform to the American Concrete Institute's (ACI) prescriptions for lap splices (2011). All the other reinforcement consisted of Grade 60, #4 bars; therefore, a standard wall had #4 bars spaced at about 12 in on center for the vertical cores and #4 bars spaced 16 in on center for the vertical cores. Contrary to standard building practices, all bars were tied and centered. The only deviation to this reinforcing schedule is described in Test Matrix section (2.2).

The concrete mix used for each set of walls was designed for compressive strength of 3000 psi at 28 days and a slump of 6.5 in. The maximum nominal coarse aggregate size was 3/8-in. These specifications were in line with standard construction practices, though the actual slump varied for each set of walls. Figure 2-3 shows slump tests performed during the casting of each wall. The slump shown for the first set of walls was measured before the concrete was placed and the slump shown for the second set was measured towards the end of placement.

Figure 2-3: Slump tests for the first set (left) and second set (right) of walls.

For the first set of walls, by the time the truck arrived, the mix was deemed too stiff to pump into the walls. Water was added in an effort to increase the workability of the mix, but too much was added, resulting in a slump of 9.25 in. The American Society for Testing and Materials standard for testing slump (ASTM C143) states that mixes with slumps greater than nine inches “may not be adequately cohesive for this test to have

significance (2012).” Fortunately, the 28-day compressive strength of the mix was as specified, but the plasticity of the mix may have caused some problems when placing concrete in the walls.

For the second set of walls, formwork was used for every wall, regardless of whether the blocks were split or not – some blocks were split in order to facilitate the removal of the ICFs from the walls which were to be tested without ICFs in place. The primary reason for constructing this formwork was so that bond beams could be formed on top of the walls. The need for bond beams is discussed in the Test Matrix section. Once again, the walls were spaced as closely as the foundation blocks would allow so that the walls were reacting both against one another and against exterior bracing. Each wall was cast in several lifts to ensure the forms were holding and so that no wall, if the forms failed, would be able to react too aggressively on a neighboring wall. Unfortunately, the slump of the mix was not measured until casting of the walls was nearly complete. The mix likely stiffened during the course of pumping the concrete, and the final measured slump was too low for this application. This issue could have been ameliorated if a concrete vibrator with an appropriate length had been used to consolidate the concrete, but all that was available (and used) was a two-foot vibrator and a long piece of #4 bar for rodding. No issues occurred when the walls were cast, but suspicions of poor consolidation were confirmed when the first wall forms were taken off of the walls in which only the reinforced concrete cores were to be tested. The voids were filled with quick setting, high-strength, non-shrink grout at least one week prior to testing.

In order to connect the walls to the load beams, 7/8-in-diameter bent anchor bolts were cast into the top of each vertical core of the walls. Each bolt was 12 in long and made from 55 ksi steel. For the first set of walls, wire mesh cages were placed around each bolt for confinement. The need for confinement was less of a concern for the second set of walls, which had 3.5-in thick bond beams. For this set of walls, the bolts were simply tied between two pieces of #3 reinforcing bar.

For the purposes of this paper, the web refers to the portion of the block that separates the vertical cores. Because of the different web thicknesses (2.25 in within the blocks and about 4 in at the joints), the vertical cores were not perfectly aligned. Figure 2-4 shows two 4-ft-long walls, one with forms to show the stacking pattern and one with the forms removed to illustrate the alignment of the vertical cores. Also, referring back to Figure 2-2, the shorter end blocks are formed as one at the plant and separated as needed in the field. The alignment of the block (labeled AP-Wallform in the figure) was such that, when cut apart, the ends of the blocks had different thicknesses – 2 in for the female block (left) and about 1.5 in for the male block (right). This discrepancy also led to some misalignment of the vertical cores.

Figure 2-4: Four-foot walls with (left) and without (right) wall forms.

.

2.2. **Test Matrix**

The test matrix was developed to consider several variables: aspect ratio, performance of the walls with and without wall forms in place, and the effect of gravity loading on wall performance. Aspect ratio was considered in an effort to have walls with both flexure-dominated and shear-dominated failures. For this procedure, aspect ratio was considered the ratio of height, which was measured from the base of the wall to the centerline of the actuator, to length for each wall. For the first set of walls, the two aspect ratios were 1.98:1 and 0.99:1, where the walls were 48 in and 96 in long, respectively, and the height to the centerline of the actuator was 95 in. Due to several unforeseen circumstances (discussed below), the test setup was changed for the next set of walls, as were the walls and the aspect ratios themselves. The first set of walls consisted of only blocks and the walls were 80 in tall (ten layers of wall forms). The actuator was

connected to a steel load beam, which would connect to the wall via the J-bolts that had been cast into the vertical cores of the wall. Several of the walls in this set were deemed to have failed prematurely and uncharacteristically when separation occurred between the top layer of blocks and the layer immediately underneath. In order to avoid this type of failure, the next set of walls were constructed with 3.5-in-thick bond beams on top of the top layer of wall forms. Because there were also problems with bending in the load beam, a new load beam was designed and fabricated so that the line of action of the actuator was in plane with the top of the wall. Therefore, the aspect ratios for the second set of walls were 1.74:1 and 0.87:1 for walls that were 48 in and 96 in long, respectively, and where load was applied at a height of 83.5 in.

Current practice dictates that only the reinforced concrete cores be considered when designing structures with the Faswall wall form. The research of Dusicka et al. (2011) and Werner (2010) suggests that the wall forms could significantly contribute to the load resistance and deformation capacity of the wall system in which they were used. In an effort to support this hypothesis, and to quantify whatever contribution the wall forms had, each aspect ratio was tested with and without the ICF blocks in place.

Previous research (Dusicka et al. 2011) had also shown that walls tested under self-weight only produced conservative results with regard to load resistance and drift capacity. In order to test this theory, and to see how the Faswall walls might perform in a commercial application, each aspect ratio was subjected to a constant 10 kip-per-lineal-foot (klf) gravity load (in addition to being tested only under self-weight) during the loading protocol. This loading was based on theoretical design loads for a three-story

commercial building and was consistent with the loading used by Dusicka et al. (2011) and Yland (2001).

As was mentioned above, the standard reinforcement for the walls tested in this procedure were #4 bars placed 16 in on center for the horizontal cores and placed 12 in on center for the vertical cores; however, in practice, vertical reinforcing is only placed in every other core (24 in on center) for walls built above grade and the detail used as the baseline for this procedure is standard for walls built below grade. One long wall (smaller aspect ratio wall) was constructed with this reinforcing detail, with the bars tied, in order to compare the performance of walls built above and below grade.

The complete test matrix is shown in Table 2-1. The wall with designation SWG was the only wall from the first set that was both tested to failure and had a reasonable failure mechanism. For these reasons, SWG was the only wall from that set that will be considered in this report. For the Gravity Loading column, SW refers to self-weight.

Table 2-1: Test matrix and designations for each wall test.

Designation	Aspect Ratio	Length (ft)	Wall Forms in Place	Vertical Reinforcement (in., OC)	Gravity Loading
LWS	0.87	8	Yes	12	SW
LWA	0.87	8	Yes	24	SW
LWC	0.87	8	No	12	SW
LWG	0.87	8	Yes	12	10 klf
SWS	1.74	4	Yes	12	SW
SWC	1.74	4	No	12	SW
SWG	1.98	4	Yes	12	10 klf

For the sake of clarity, the different types of walls (along with their designations) are shown in Figure 2-5. Each specimen designation comprised three letters. The first two (LW or SW) signify whether the specimen is a long wall or a short wall. The third letter indicates whether the specimen was a standard wall (S for standard), had vertical reinforcing in alternating cores (A for alternate), had the ICFs removed (C for core-only), or was subjected to a 10 klf gravity load (G for gravity loading).

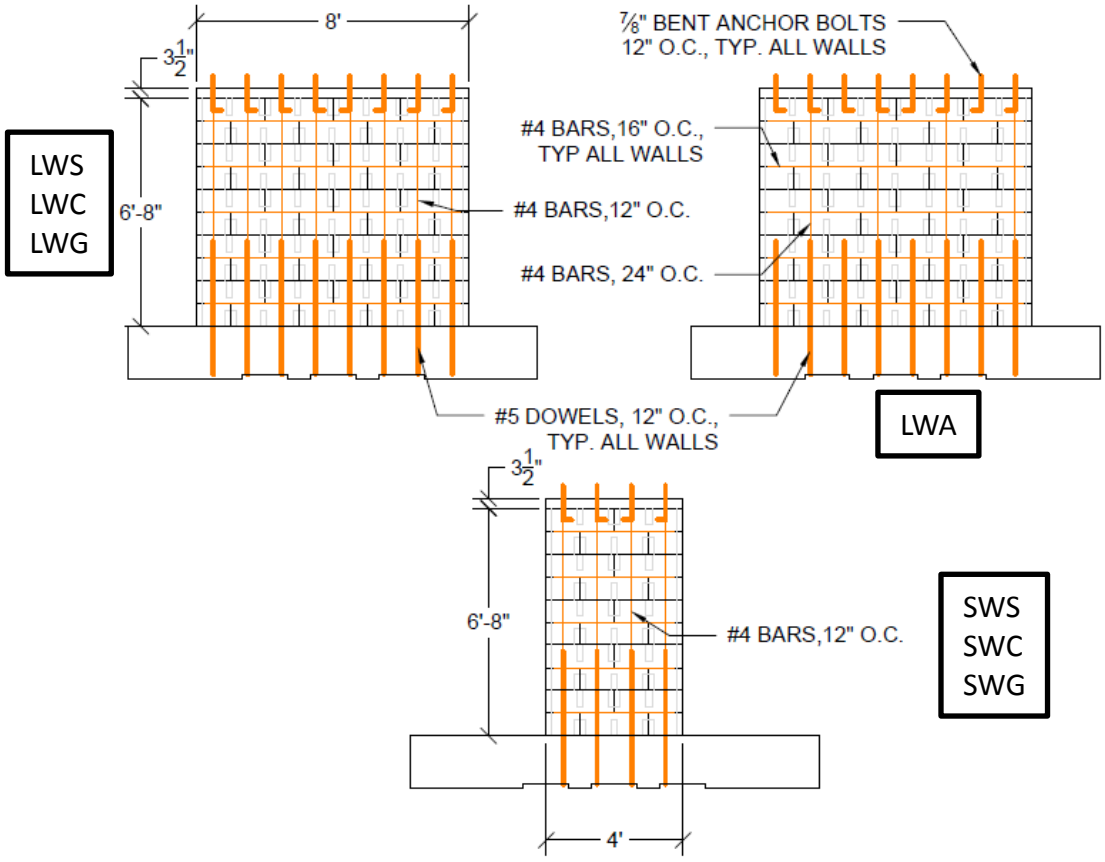

Figure 2-5: Schematic of wall types.

2.3. **Foundation Blocks**

The need for reusable foundation blocks arose from both the spatial constraints of the lab and the desire to have some flexibility in the amount of walls to be tested. Figure

2-6 shows a partial reinforcing detail of the blocks. The blocks were conservatively designed in the hopes that any failure that occurred during testing would be limited to the walls themselves. The conservative design was based on the assumption that all dowels (#5 bars, Grade 60) would yield simultaneously and that the walls would withstand a lateral load that was twice the capacity of the actuator's load cell (200 kips). The blocks were clamped to the lab's strong floor with HSSs spaced at 260 cm (with the walls centered between each HSS), so the blocks were assumed to be simply-supported at these locations. The longitudinal reinforcement was the same for the top and the bottom of the floor beams and consisted of four #7 bars placed, two on either side of the ducts, and two #6 bars between the ducts. The transverse reinforcement consisted of #4 hoops that were doubled-up (four total legs) in the regions outside of the ducts and, due to limited space, single #4 hoops between the ducts. Given the spatial constraints of the reinforcement/ducts and that the blocks were being cast before the walls, the same mix that was eventually specified for each set of walls was used for the blocks. Unlike the walls, no pump was used and the slump was within a quarter-inch of the specification – between 6.5 and 6.75 in.

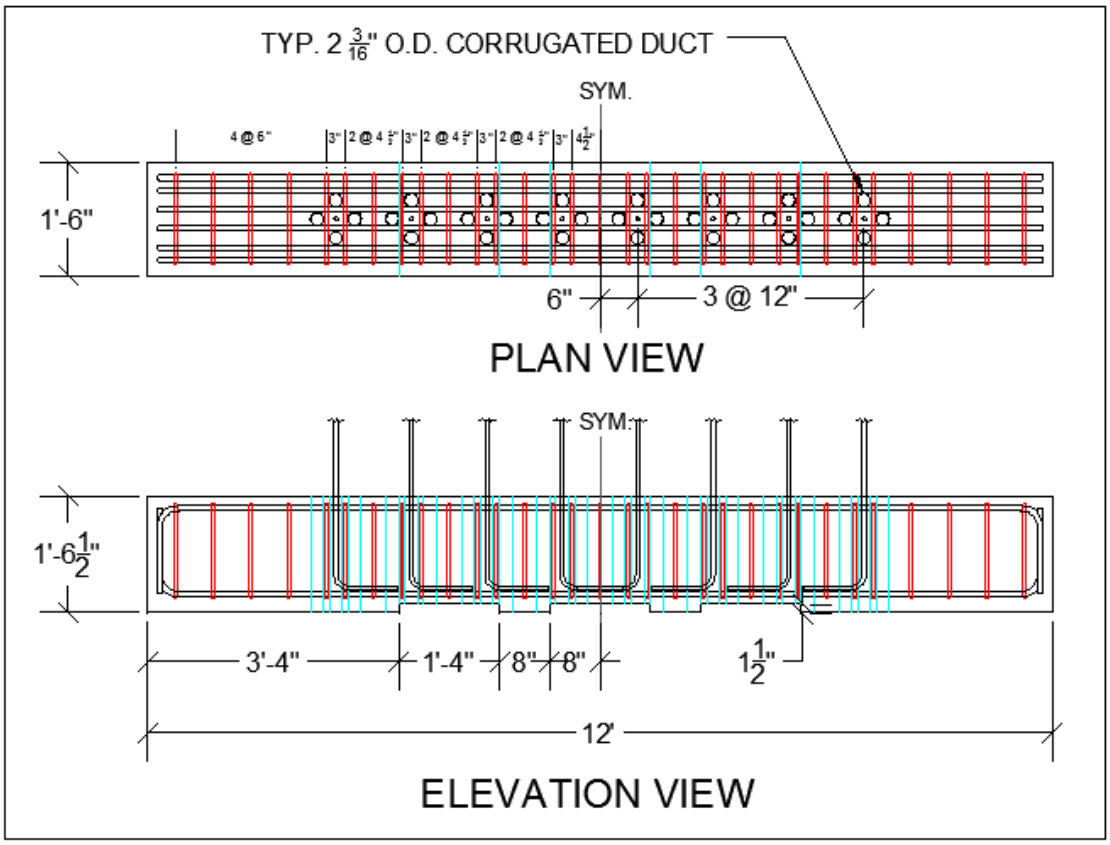

Figure 2-6: Reusable foundation block detail.

In order to make the blocks reusable, a system had to be developed to insert future sets of dowels such that the bars (#5, Grade 60) could at least reach yielding before pulling out. After some deliberation, the system decided upon consisted of using straight bars in corrugated post-tensioning ducts with non-shrink, high strength grout. This decision and the determination of the size of ducts were based on the research conducted by Raynor, et al. (2002). The main conclusion drawn from this paper was that a straight reinforcing bar can reach failure in tension with a significantly smaller development length in a grouted duct than is possible in standard concrete. In order to verify this

research and the assumptions made for scaling down the bar and duct sizes, a pullout test was performed, the results of which are discussed below.

The final consideration made with respect to the design of the blocks was how to utilize them as part of the gravity loading system. As is discussed later, the blocks were designed to facilitate U-shaped steel brackets at multiple positions, depending on aspect ratio and wall placement. Three gaps underneath the block can be seen in the elevation view of Figure 2-6. These gaps were designed so that the U-shaped brackets could be placed under the blocks and bear upon the bottom of the blocks when the gravity load was applied.

2.4. **Loading Protocol**

This procedure utilized the same loading protocol as both Dusicka et al. (2011) and Werner (2010). This protocol was based on recommendations by the ACI for testing unbonded post-tensioned precast shear walls (2008) and moment frames (2001). The protocol was displacement-controlled, fully-reversed, and quasi-static. The initial drift ratio (as recommended by both of these ACI documents) was selected to be well within the wall system's linear elastic range. For the sake of comparison, the initial value of 0.07% drift, which was used in Dusicka et al, was used for this procedure. Three fully-reversed cycles were conducted for each drift, and subsequent drifts were increased by a factor of 1.4. Both ACI reports specify that the step factor used to increase the drift should be between 1.25 and 1.5 in order to avoid premature degradation of the specimen due to too many low-level cycles and so that the deformation capacity can be reasonably measured, respectively (ACI 2001, 2008). When reviewing the protocol used in Dusicka,

et al., it was determined that an intermediate step of 3.47% was placed between the drifts of 2.89% and 4.05%. For the sake of consistency, this step was included in the protocol for this procedure. This intermediate step, while failing to exceed the minimum 1.25 step factor prescribed by the ACI reports, does conform to the specification in ACI T1.101 (for moment frames) that the drift be taken up to or beyond 3.5% (2001). A graphical representation of the load protocol is shown in Figure 2-7. For the sake of consistency, the forward, or positive, direction for each cycle corresponded to the outward displacement of the actuator, while the reversed, or negative, direction for each cycle was associated with the inward displacement of the actuator's piston.

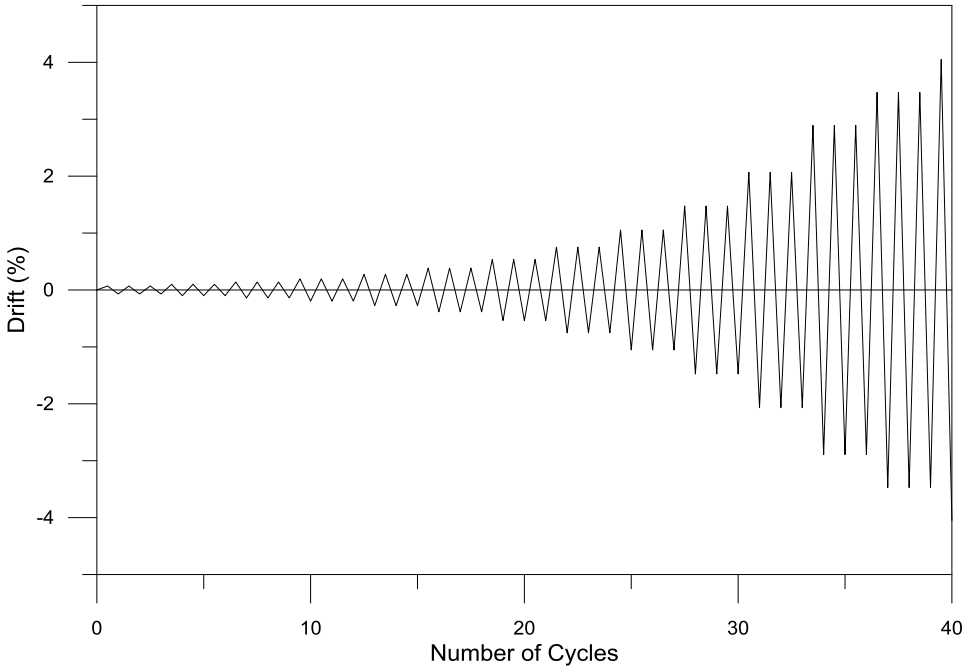

Figure 2-7: Fully-reversed cyclic loading protocol.

2.5. **Testing System and Instrumentation**

As was previously mentioned, two different load application systems were used throughout the course of testing. The first system is shown in Figure 2-8. As can be seen

in the two photographs at the bottom of the figure, two angles were added to the load transfer beam in an effort to reduce the bending in the W-section that was induced whenever any load was applied by the actuator. Out-of-plane issues with the last set of ICF tests performed at PSU (Dusicka et al. 2011) led to the design of this load beam. The front-loaded beam, in conjunction with inadequate lateral bracing, caused rotation and out-of-plane displacement in some of the walls. The primary goal of the (first) design for this setup was to line up the in-plane centerline of the wall more closely to the centerline of the actuator in order to reduce as much potential out-of-plane motion as possible, in case the lateral bracing system proved to be inadequate. Two 13-ft pin-pin links were used for lateral bracing in each testing system. Eight holes were drilled into the web of the W-section in order to connect the load beam to the anchor bolts that were cast into each set of walls. These holes were positioned on the beam to be aligned with the line of action of the actuator. In this way, because of the asymmetry of the blocks caused by insulation being placed on one side of the core, load was applied to the centerline of the reinforced concrete cores, not the walls themselves. Three sets of double angles were welded in the transverse direction in order to cradle the hydraulic rams that were used to induce axial loads on the walls.

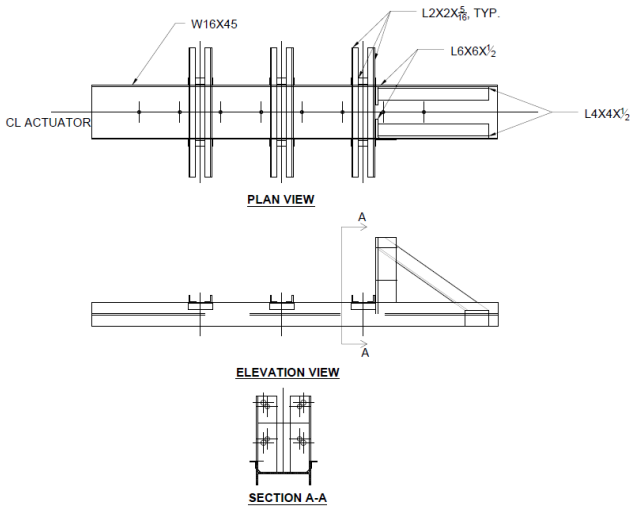

Figure 2-8: Specifications for the first load beam.

The first test conducted was on the long wall (without additional gravity loading) shown in Figure 2-9. Once the bending issues in the W-section were noticed, testing was terminated and the extra angles were welded into place. The angles were meant to help the W-section resist some of the rotation induced by loading and, when testing was resumed, they appeared to help, but some bending was still visible. In addition to the bending in the load beam, a new problem had arisen: the uppermost end blocks were separating from the rest of the wall. Testing was then cancelled as the failure was deemed unrepresentative for the wall. The system was tried again using both short walls without additional gravity loading and the results were the same as the long wall: failure due to separation of the uppermost cores from the rest of the wall. The system was used for the short wall with additional gravity loading, and a more reasonable failure mode: deterioration of the horizontal cores and softening at the lap splice. Due to some construction problems, the two remaining walls were unsuitable for testing. The combination of bending in the load beam and the unrepresentative failures seen in the

walls without additional gravity loading led to the implementation of both a new load transfer beam and a reinforced concrete bond beam on top of the wall.

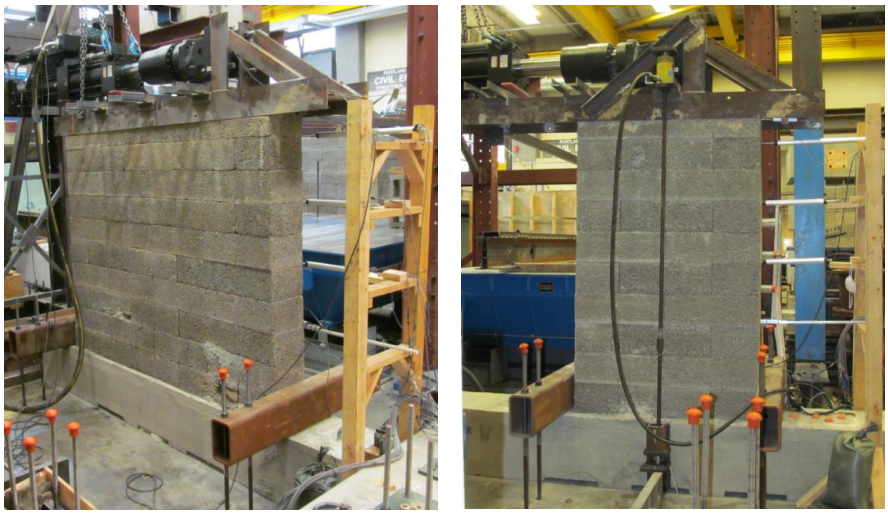

Figure 2-9: Long wall without gravity loading (left) and short wall with gravity loading (right).

The second load beam consisted of a W16x45 section that was 98.38 in long with a 1.5-in thick plate welded to the front to connect to the actuator. A portion of the fabrication drawing is shown in Figure 2-10. Other than the point of load application, the major differences between this load beam and the first were the alignment of the holes for the anchor bolts and the sections used to support the hydraulic rams. The realignment of the holes meant that the line of action of the actuator was collinear with the centerline of the wall, not the reinforced concrete cores. The eccentricity (1.5 in) of the load path through the cores was judged to be reasonable since load would be transferred to a wall via the concrete bond beam. This realignment also gave the insulation-side flange more clearance from the wall, which had been a slight issue with the previous load beam. The

hollow structural sections (HSSs) were used because the moment resisting capabilities needed to be increased as a result of the realignment of the holes.

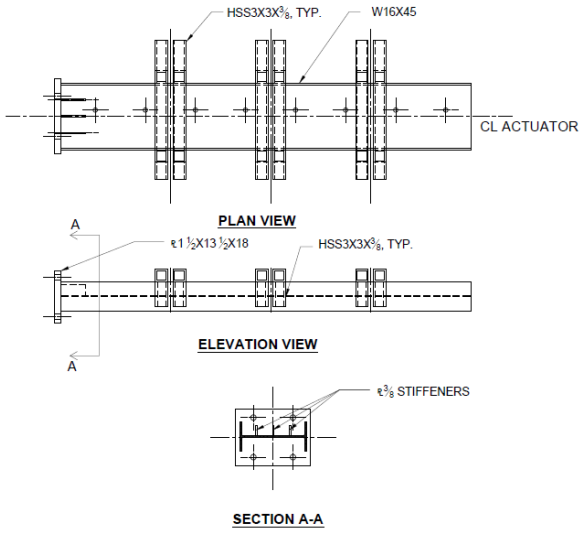

Figure 2-10: Detail of second load beam.

Figure 2-11: Long wall with second load beam and additional gravity load applied.

The drift-controlled loading protocol was executed using a 110-kip hydraulic actuator with a static stroke of ± 11 in, which was measured by an internal linear variable differential transformer (LVDT). This actuator was equipped with a 100-kip capacity load cell, which was used to measure the load-resistance of the walls. A total of 14 additional LVDTs were used to measure a variety of displacements that the wall, foundation block, and load beam were expected to experience. Figure 2-12 shows a schematic of the test setup and the positioning of each LVDT.

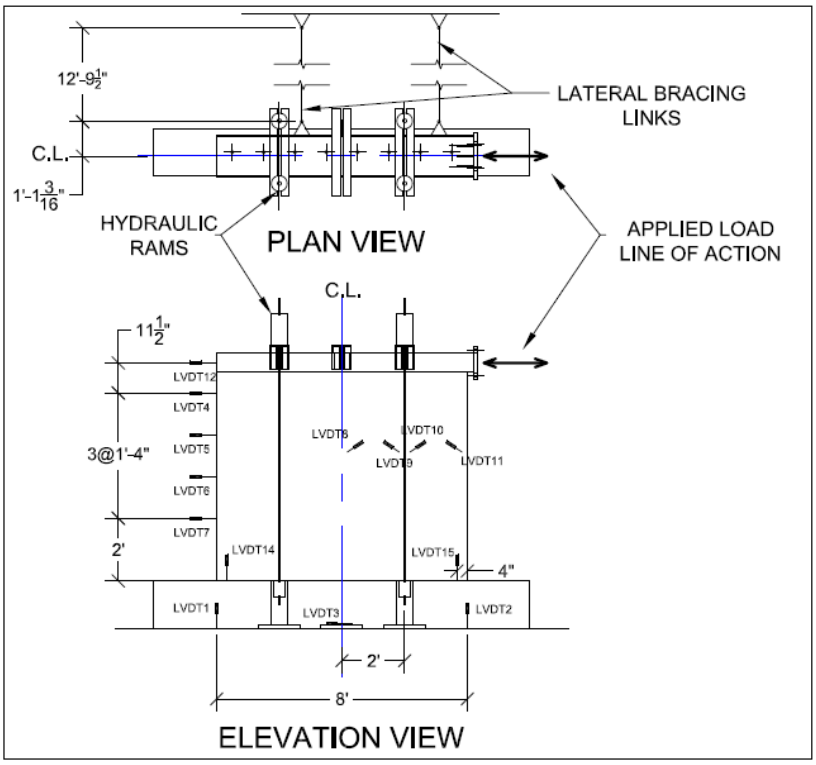

Figure 2-12: Instrumentation and test setup.

Three LVDTs were placed on the foundation block in order to verify that no slipping (LVDT3) or uplift (LVDTs 1 and 2) was occurring between the block and the strong floor. One LVDT (12) was used to measure the relative displacement between the load beam and the top of the wall. Four LVDTs (4- 7) were used to measure the displacement at different heights of the wall that corresponded with the locations of the horizontal cores. Four LVDTS (8-11) were placed diagonally on the wall to measure the shear deformation between vertical cores. These LVDTs were connected to swiveling brackets and had wires tied to their pistons which were tied to masonry screws lodged into the vertical core to the left or right (depending on the LVDT) of the core on which

the LVDT was situated. Figure 2-13 shows a close-up of LVDTs 10 and 11 for one test. Finally, two LVDTs (14 and 15) were used to measure uplift at the ends of the walls.

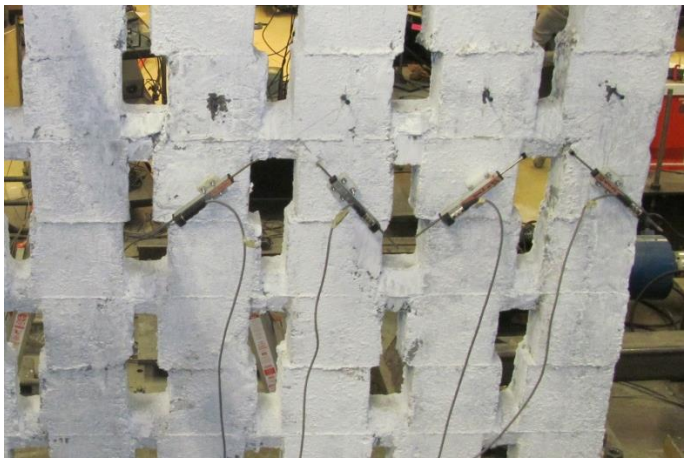

Figure 2-13: LVDTs measuring shear deformation between cores.

During testing, the loading protocol was executed by inputting the desired drift into the controller for the actuator. Actual drift was measured by subtracting the total system slip from the actuator's measured displacement. This corrected drift value was displayed on the virtual interface of the data collection software and was subsequently used to determine the remaining distance the actuator needed to displace in order to reach the target drift. This value was also to anticipate slip for subsequent cycles, in order to prevent starting and stopping the actuator multiple times during the course of reaching a target drift.

In order to provide 10 klf of axial load, hydraulic rams – either two or four, depending on the length of the wall – were used and kept at (mostly) constant pressure. The rams were connected to a single pump with a splitter and an analog gauge, which was attached to the line between the pump and the splitter. The pistons in the rams were

allowed to protrude several inches before they engaged so that when higher lateral loads were achieved there was no risk of the pistons fully retracting while trying to maintain pressure. Each ram was responsible for 20 kips of the load and two 100-kip load cells were used to ensure that the load remained constant. At higher displacement levels, the pressure would be reduced drastically once the wall was brought back to the zero position. The pump would be jogged in these circumstances in order to bring the pressure back up to the desired value. The axial load system can be seen in Figure 2-11 and Figure 2-12.

Chapter 3: MATERIAL TESTS

3.1. **Concrete**

Two concrete cylinders were tested at seven and 28 days after placement, and on the day of each wall testing, with two exceptions: wall specimens LWS and LWA used the same cylinders (due to lack of access to the load frame that was used for cylinder tests), which were tested two days after LWS and two days before LWA. The average compressive strengths, f'_c, for each test are shown in Table 3-1.

Table 3-1: Average compressive concrete strengths.

Designation	f'_c (psi)	7-day f'_c (psi)	28-day f'_c (psi)
LWS	5463	3524	5310
LWA	5463		
LWC	6154		
LWG	5649		
SWS	6426		
SWC	6028		
SWG	4037	2036	3738

The concrete mix design for all walls specified a 28-day-strength of 3000 psi. The stiffness (i.e., the lack of water content) of the second mix was the likely culprit for driving up the strength of that mix, which was used for all walls except SWG (hence, the lower respective compressive strength for this specimen). Even with the high slump, the first mix easily exceeded the specified 28-day-strength. The standard mix design is shown in Appendix: Concrete Mix Design

3.2. **Steel**

Table 3-2 shows the results of the tensile tests performed on the reinforcing used in each wall. The results shown are the averages of values obtained for two different samples. The only exceptions are the values marked by an asterisk. Data collection did not begin for the first sample until after yielding had occurred. For each set of walls (SWG was part of the first set, all others made up the second set), each type of bar (e.g., #4 or #5) was specified to be Grade 60 and from the same batch. The difference between some of the #4 bars in the second set was the result of some miscommunication with the vendor, such that more rebar, which was inevitably from a different batch, had to be ordered.

Table 3-2: Average yield and ultimate strengths for steel reinforcing.

Specimen	#5 Bars		#4 Bars (Horizontal)		#4 Bars (Vertical)	
	f_y (ksi)	f_u (ksi)	f_y (ksi)	f_u (ksi)	f_y (ksi)	f_u (ksi)
LWS	75.9*	107	80.0	116	80.0	116
LWA	75.9*	107	80.0	116	77.1	111
LWC	75.9*	107	80.0	116	77.1	111
LWG	75.9*	107	80.0	116	80.0	116
SWS	75.9*	107	80.0	116	80.0	116
SWC	75.9*	107	80.0	116	77.1	111
SWG	74.1	109	73.6	106	73.6	106

*Value is for one sample, not two.

3.3. **Pullout**

A test was needed to make sure the #5 bars that were placed in the grouted ducts would be able to reach yielding before pulling out of the ducts. In order to perform this test, an extra piece of 60 ksi reinforcing bar was placed in an open grouted duct in the same manner as the rest of the dowels. After the short wall that shared a foundation block

with this specimen was tested, the setup for the pullout test was put together. This setup is shown in Figure 3-1.

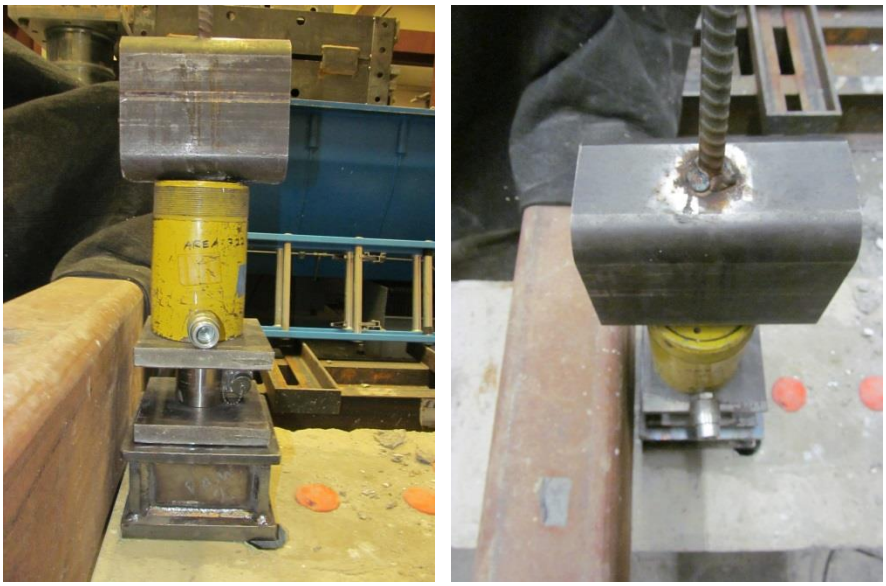

Figure 3-1: Rebar pullout test setup.

The test setup consisted of a steel levelling base (which was designed to be used with a hydraulic ram to post-tension the steel rods that fasten objects to the strong floor), two 1-in-thick plates, a 100-kip load cell, a 30-ton hydraulic ram, and a six-inch length of HSS4x6x1/2. The HSS had a hole drilled through the top and bottom in order to put the bar through it such that the four-inch side would be reacting against the ram and the rest of the system underneath. The bar was then welded to the top of the HSS around the hole. The bar, not surprisingly, failed at the weld, but at a load of about 32.7 kips. At this load, the stress in the bar reached 105.5 ksi, which was 76% higher than the specified yield strength of the bar and 99% of the average ultimate capacity of the sample bars (the #5 bars for all walls but SWG in Table 3-2).

Chapter 4: TEST RESULTS AND OBSERVATIONS

Each wall was brought to failure using the same loading protocol and assuming the same criterion for failure, i.e., when, after peak load had been reached, the load resisted by the wall was less than or equal to 80% of the peak load. The drift at which this event occurred was considered to be maximum drift or the deformation capacity of the wall.

4.1. Long Walls

The failure modes for each of the long walls seemed to follow a similar pattern. For the walls that were tested with the forms left in place (LWA, LWG, and LWS), there was some difficulty in ascertaining what was occurring inside the wall forms until the later cycles, when the forms started falling off of the reinforced concrete grid. The specimen that had the wall forms removed (LWC) offered some insight into what was taking place to each wall during the lower level cycles.

4.1.1. LWC

Figure 4-1 shows specimen LWC after undergoing four different levels of the protocol. Shear cracks became visible in the horizontal cores of LWC after the first set of cycles at 0.54% drift. In addition to the cracking in the horizontal cores, flexural cracking had begun in some of the vertical cores. The wall's peak load resistance (in both directions) was realized during the primary cycle at 0.75% drift. Peak positive load was 38.0 kips and peak negative load was 41.0 kips. The next significant events occurred at 1.05% drift when some of the horizontal cores started falling apart and when a large shear

crack appeared in one of the vertical cores. The subsequent set of cycles (1.48% target drift) saw the proliferation of the previously formed cracks as well as the development of several flexural cracks in the vertical cores around the end of the lap splice and below the uppermost set of horizontal cores and several more diagonal cracks in the vertical cores, between the regions where the horizontal cracks were forming. For the remainder of the loading protocol, the cracked region at the level of the lap splice (approximately 30 in above the foundation block) essentially acted as a hinge – the region below this "hinge" moved very little with respect to the region above. Technically speaking, the wall had failed in the reverse direction under this set of cycles as the load resistance fell below 80% of the peak. But, the resistance in this direction had only fallen by 23% (versus the allowable 20%) while resistance in the forward, or positive, direction had only fallen by 19%. Testing continued, and the load resistance of the wall stayed relatively constant in both directions for the next two target drifts, which were 2.07% and 2.89%. At 2.89% target drift, the cracked region below the top row of horizontal cores began to act as a hinge and the wall's ability to withstand lateral load dropped 28% and 25% below peak load in the positive and negative directions, respectively. This portion of the loading protocol also caused the catastrophic failure that occurred in the upper region of the vertical core that is second from the left in Figure 4-1.

(a) 0.00% Drift

(b) 1.05% Drift

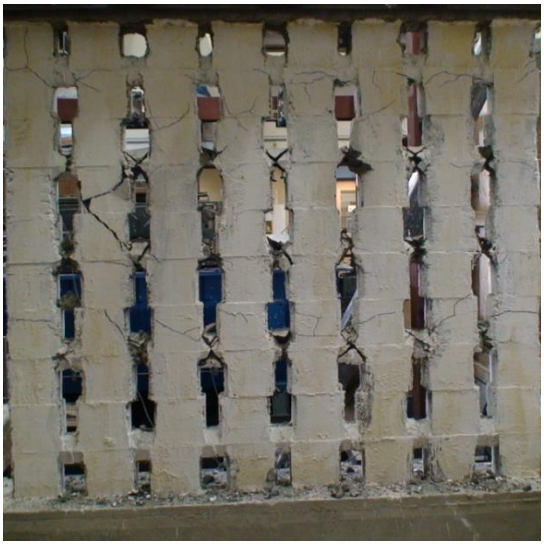

(c) 2.07% Drift

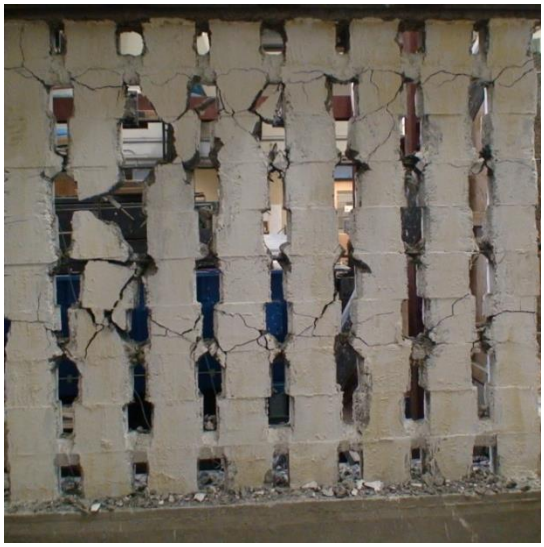

(d) 4.05% Drift

Figure 4-1: Specimen LWC after noted drifts.

4.1.2. LWA and LWS

Figure 4-2 shows selected drifts from the test of specimen LWA. The first visible sign of damage in walls LWA and LWS was separation between the mid-height, tension-side end blocks at 1.05% drift. This region roughly corresponds to the height of the lap splice – the blocks were 8 in tall, so four blocks from the foundation would be 32 in, while the height of the #5 dowels was 30 in. A similar, but far less pronounced phenomenon occurred in specimen LWG (i.e., the wall that was subjected to additional gravity loading) at this drift, but only for the forward duration of the cycle. In addition to the separation of the end blocks in LWA and LWS, diagonal cracks became visible on the back side of each wall in the mid-level ICFs. For reference, the front side of the wall refers to the face that is shown in Figure 4-2 and for all tests conducted with the ICFs in place. This side of the wall corresponded to the side of the wall forms where the insulation was located; therefore, the interior of a block on the back side of the wall was in direct contact with the concrete cores. Specimen LWC only had faint flexural (horizontal) cracks in this region at this drift; however, at this point in the loading protocol, the three central horizontal cores of LWC had already undergone significant diagonal shear cracking. At target drift 1.48%, vertical cracking was visible on the front side end blocks for these specimens. These cracks can be better seen in Figure 4-3, which shows specimen LWS after a couple of target drifts. As testing progressed to higher drift levels for walls LWA and LWS, the separation in the end blocks and the shear cracking in the blocks on the back side of the wall became more pronounced. Figure 4-4 shows two examples of the cracking that occurred in the back side of wall LWS. At 2.07%, the ICFs appeared to be separating in a diagonal or zigzag pattern, as can be seen in Figure

4-2(c). Each of the forms of damage continued to progress until failure was reached. Walls LWA and LWS both reached failure during the cycle course with a target drift of 3.47%.

(a) 0.54%

(b) 1.48% (+)

(c) 2.07% (-)

(d) 3.47%

Figure 4-2: Progression of test on specimen LWA at (or after) the drifts specified.

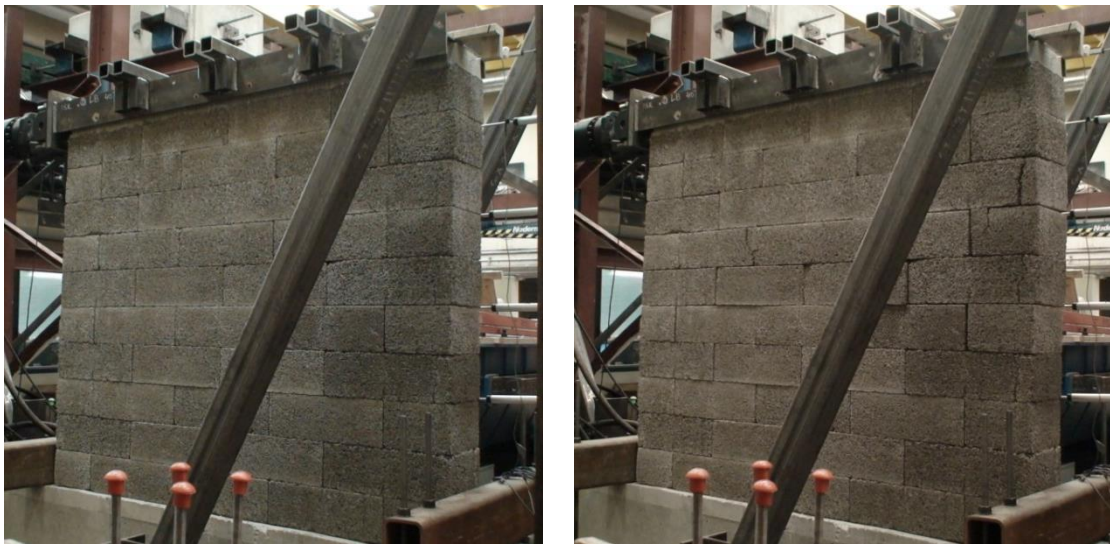

1.48% Drift 2.89% Drift

Figure 4-3: Specimen LWS after the specified target drifts.

2.07% Drift 2.89% Drift

Figure 4-4: Cracking in the forms on the back side of specimen LWS.

Posttest inspections showed that both walls had experienced significant damage in the horizontal cores as well as pronounced shear and flexural cracking in the vertical cores. The primary flexural cracking appeared to be between the fifth and sixth blocks

(for both walls), which would be about 10 in above the lab splice. Wall deflection data for LWS showed that hinging occurred well below that region when the wall was displaced in the positive direction. When the wall was displaced in the negative direction, hinging appeared to occur 40 in above the foundation block, or where major flexural cracking was most apparent. The same data were inconclusive for wall LWA because of the end block (on the right, fifth from the foundation block) that popped out of place during the cycle sequence at 2.89% target drift, as can be seen in Figure 4-2. Figure 4-5 shows both walls after failure with wall forms removed from critical regions. While removing these wall forms, extra care was taken to not disturb the interior cores, but loose pieces of concrete were inevitable after the walls had been tested to failure.

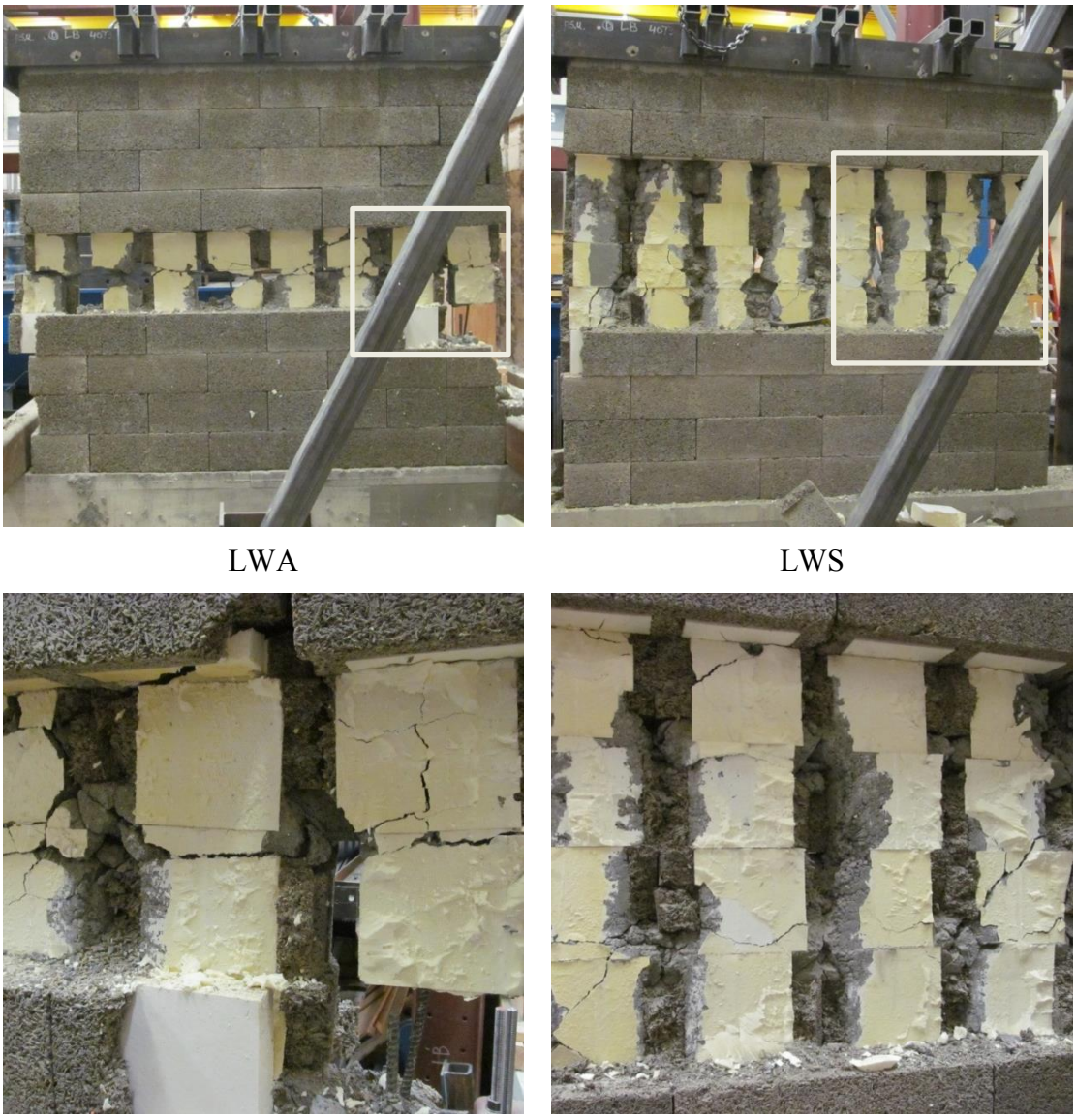

LWA LWS

LWA (Right End) LWS (Middle)

Figure 4-5: Walls LWA and LWS after testing sequence was completed.

4.1.3. LWG

The progression of testing for specimen LWG is shown in Figure 4-6. Unlike the other long walls, no perceived visible damage had occurred to this specimen until after the 2.07% target drift sequence. Even though there had been slight separation between the end blocks during earlier cycles, this phenomenon was not obvious until after the full

protocol had been executed and the photographs taken during testing had been thoroughly examined.

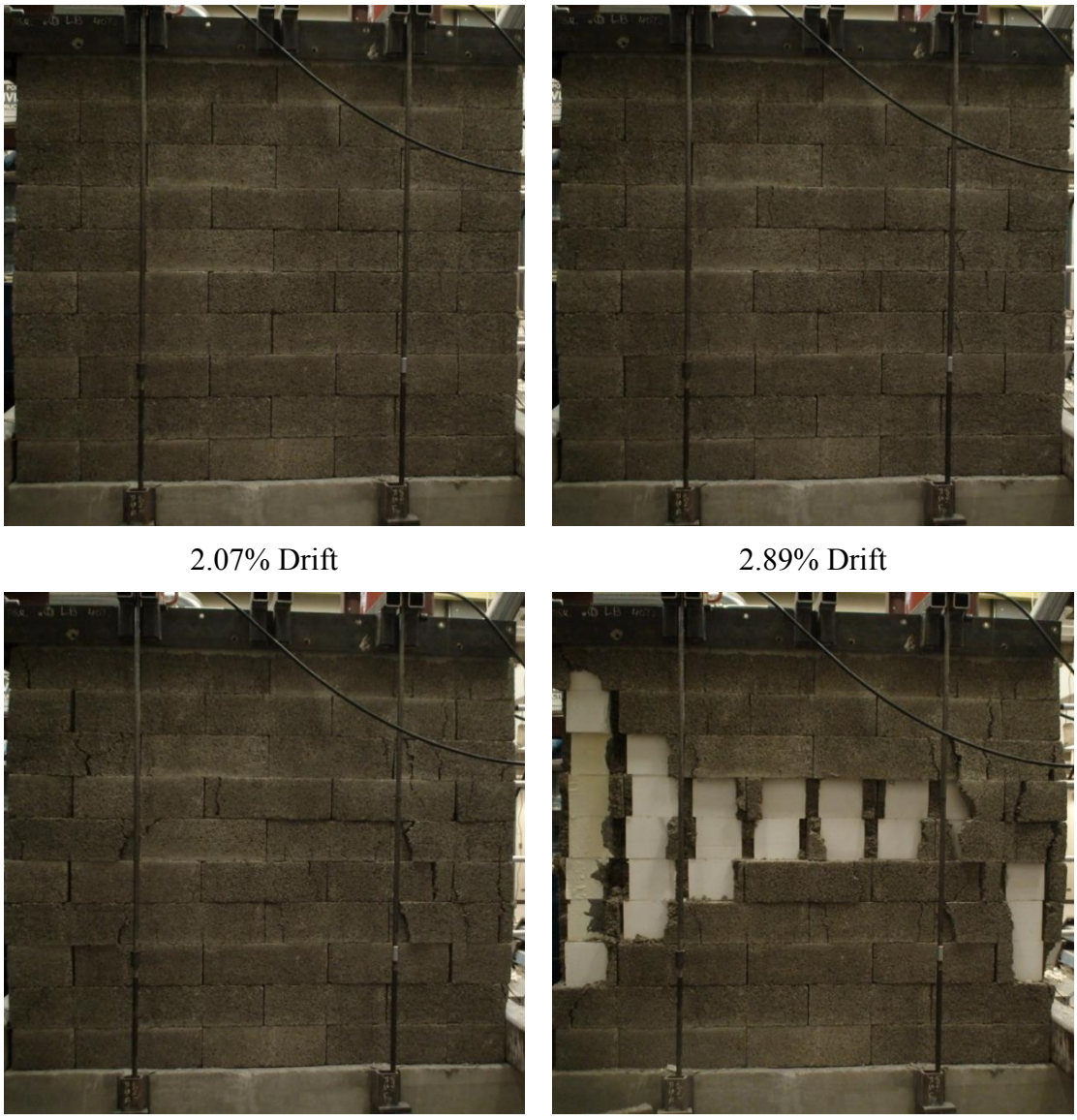

2.07% Drift 2.89% Drift

3.47% Drift 4.05% Drift

Figure 4-6: Progression of testing for wall LWG.

At 2.07% drift, vertical cracks were noticed in several wall forms on the front side of the wall. These cracks continued to propagate while similar cracks formed and propagated over the next two set of cycles. At 3.47% drift, some of the forms were protruding from the wall. Testing was stopped after a full set of cycles at a target drift of 4.05%. During this sequence, a fair number of forms sheared off from their webs and fell to the floor. On the back side of the wall, there were both vertical and diagonal cracks in the wall forms that seemed to form in any area where there was a horizontal core. These cracks were first observed at 2.07% target drift and continued to propagate until testing was terminated. Though cracking in this area was severe, and some forms had begun to dislodge, at the end of the test, all forms were still clinging to this side of the wall. This wall did not reach peak load resistance until a drift of 2.91%, on average. The average deformation capacity of this wall was 3.60%.

After testing was completed, the wall forms were removed from the specimen in order to inspect the damage incurred by the internal reinforced concrete grid. As was the case with the previous walls, the interior horizontal cores (i.e., the three middle rows) had all been either completely or almost completely sheared off. Unlike the other walls, there was no major flexural cracking in the vertical cores, not even around the lap splice. The vertical cores did experience significant diagonal shear cracking and some vertical cracking that seemed to propagate from shear cracks. Figure 4-7 shows a picture of the wall upon inspection. The latter cracking phenomenon is visible in the upper and lower portions of the vertical core that is furthest to the right.

Figure 4-7: Specimen LWG after loading protocol.

Long Wall Summary

The hysteresis curves are displayed in Figure 4-8 for each wall with an aspect ratio of 0.87:1. The graphs have the same set of axes for the sake of comparison. A cursory glance at each graph, and at the graphs as a group, confirms the basic expectations of wall performance. In general, each hysteresis is fairly symmetric, i.e., each wall seemed to have resisted a similar amount of load in each direction for each set of cycles. The only real exception to this was specimen LWA, which was somewhat expected given that only every other vertical core had reinforcement and there were an even number of cores (i.e., the reinforcement detail was not symmetric). The load resistance of LWA was still similar for forward and reverse cycles, but peak load was seen by each at different target drifts. The same was true for the wall's peak deformation

capacities. The envelope curves for each wall (solid) and for wall LWS (broken) are shown on each graph, also for the sake of comparison.

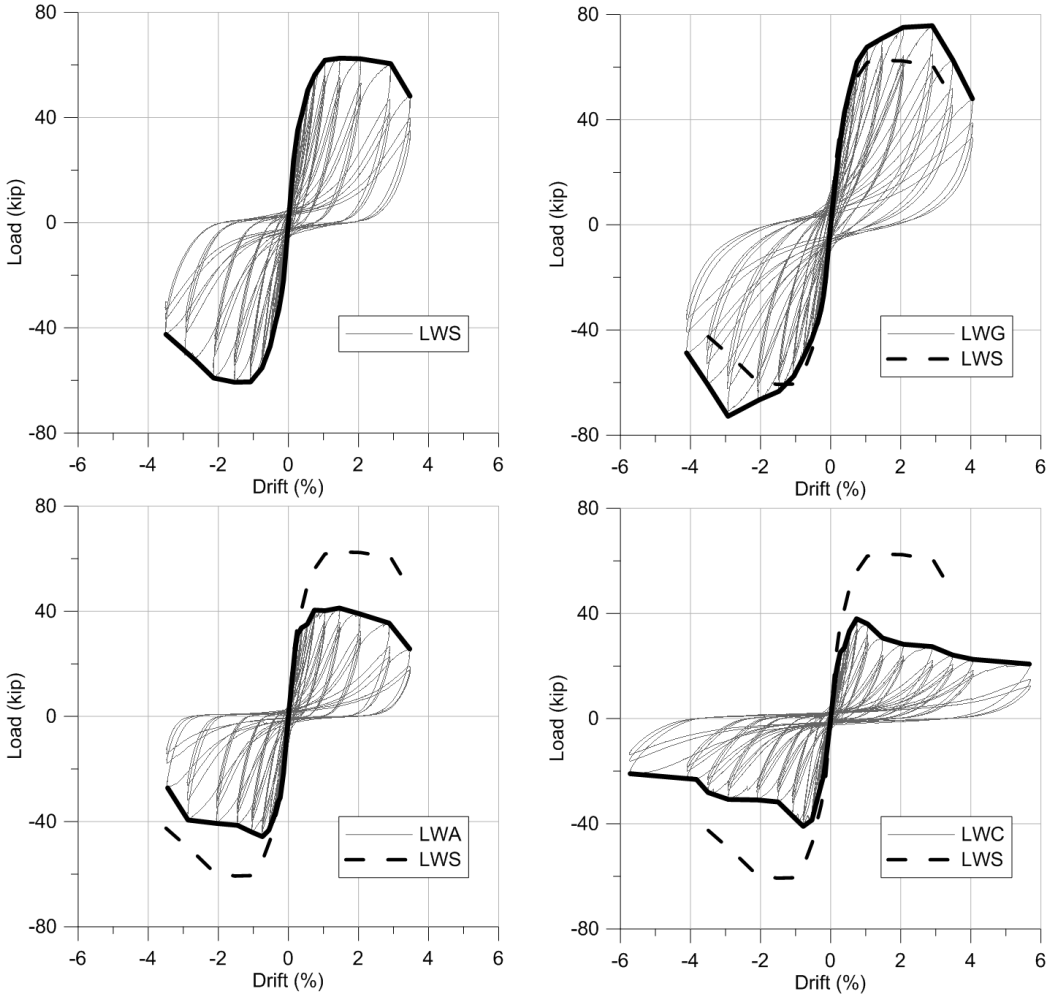

Figure 4-8: Hysteresis curves for 0.89 aspect ratio ICF walls.

Each hysteresis exhibits pinching behavior. This pinching refers to how, when the wall was being cycled at higher drifts, the load resisted by the wall approached zero as the system was approaching the initial zero deformation. This phenomenon was caused by a degradation of the specimen's initial stiffness from earlier, lower-level, cycles to such a point that the specimen can be subjected to relatively (depending on the magnitude

of the previous cycles) large amount of deformation before resisting much load. To look at the situation practically, this behavior indicates that if a structure of this type underwent a significant amount of lateral loading in the field, very little force would be required to induce large deflections in the structure. This topic will be discussed at greater length below, when the relative stiffness of each specimen is discussed.

For a more direct visual comparison, Figure 4-9 shows the backbone curves for each long wall. The backbone curves were developed by drawing lines between the peak loads of each cycle. These curves show the walls all had similar initial stiffness values during the low level cycles.

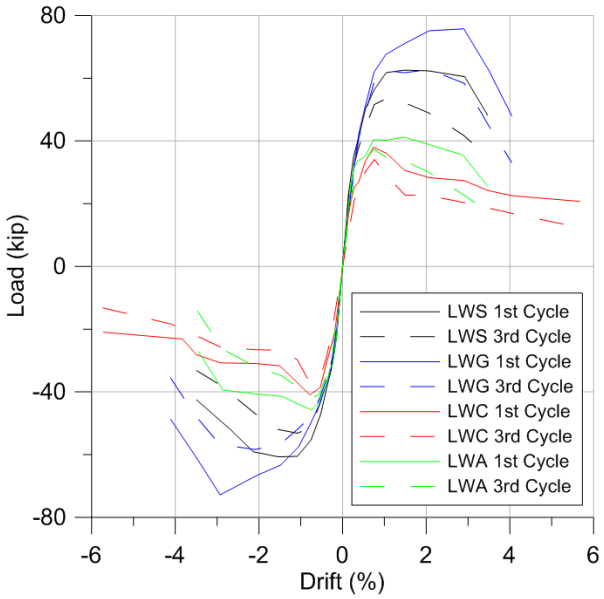

Figure 4-9: First and third cycle backbone curves for each 0.89 aspect ratio wall.

Table 4-1 shows the peak loads and deformation capacities of each wall. The peak loads are designated as V_{max} and deformation capacity is represented as Δ_u, where deformation capacity is defined as the drift on the backbone curve corresponding to a drop in load resistance to $0.8V_{max}$.

Table 4-1: Peak loads and deformations for 0.89 aspect ratio ICF walls.

Specimen	V_{max} (kips)		Δ_u		K_{eff} (kip/in)		μ	
	Forward	Reverse	Forward	Reverse	Forward	Reverse	Forward	Reverse
LWS	62.6	60.7	3.4%	3.0%	115.2	109.8	5.2	4.5
LWA	41.2	45.7	3.0%	3.0%	142.2	123.5	8.7	6.8
LWC	38.0	41.0	1.6%	1.4%	80.5	86.0	2.7	2.8
LWG	75.8	72.8	3.6%	3.6%	104.1	69.6	4.1	2.9

As was expected, based on the component tests performed by Werner (2010) and the full-scale APEX tests reported by Dusicka et al. (2011), the walls with the Faswall forms in place resisted more load than those that did not have wall forms. On average, the peak load resisted by LWS was 56% greater than the load resisted by specimen LWC. Unlike the results obtained by Werner, the wall forms also increased the ultimate drift of the walls. Specimen LWS had a deformation capacity that was, on average, 114% greater than that of LWC.

Doubling the spacing of the vertical reinforcement reduced the peak load of the wall by an average of 30%. The deformation capacity of specimen LWA, however, was only 5.4% less than that of specimen LWS.

The addition of the 10 klf gravity load increased the performance of the wall all around. Specimen LWG had an average peak load resistance that was 21% greater than that of LWS. The deformation capacity of the axially-loaded specimen was 13% greater, on average, than that of the baseline specimen.

In addition to peak loads and deformations, Table 4-1 shows the effective stiffness, K_{eff}, and ductility ratio, μ, for each wall in each direction of loading. The

ductility ratio provides some insight into the plastic deformation capacity of the wall. In order to remain consistent, these values were determined in the same manner as Dusicka et al. (2011). The envelope curves were used to develop idealized bilinear curves in order to simplify the approach. The elastic portion of the curve was defined by K_{eff}, which was a secant stiffness that ran from the origin (zero load and zero drift), through a point (before V_{max} was reached) on the envelope curve corresponding to $0.75V_{max}$. This line was extended to the value of V_{max} and the corresponding drift was referred to as Δ_y, such that Δ_y was equal to V_{max} divided by K_{eff}. The plastic portion of the curve was defined to be a line that ran from the value of V_{max} and Δ_y to the point on the envelope curve where Δ_u occurred. With the elastoplastic curve defined in this manner, the ductility ratio was determined to be Δ_u divided by Δ_y.

4.2. **Short Walls**

During the course of testing, the short walls exhibited many of the same modes of failure as their stouter analogs. This section discusses the modes of failure of each wall and provides a summary of each wall's performance under the cyclic loading protocol described above.

4.2.1. SWC

The progression of the in-plane testing on specimen SWC is shown in Figure 4-10. Like specimen LWC, the first signs of damage in this wall were shear cracking in the horizontal cores. These cracks were visible in the cores above and below the lap splice after the 0.27% target drift sequence. The next two sets of cycles caused these cracks to propagate and also caused shear cracks to form in several other horizontal

cores. After the group of cycles with a target drift of 0.75%, a flexural crack appeared on the tension side (the right side of the wall in the photos) in the reverse direction. The wall reached peak load resistance in the on the following cycle (1.05% target drift), but only displayed shear cracking in the horizontal cores, some flexural cracking in the exterior vertical cores, and some shear cracking in the interior vertical cores. At this point, no pieces of concrete, or grout, were falling from the wall. This phenomenon did not occur until the next two cycles. Hinging around the splice may have begun during the 1.05% drift cycles, but did not become pronounced until the following set of cycles was initiated. This hinging appeared to occur above the second set of horizontal cores (from the foundation block), around the region of the lap splice. The hinging was likely caused by a combination of the flexural cracks in the exterior vertical cores and the shear cracks in the interior vertical cores. At the target drift of 1.48%, the horizontal cores started shearing off and larger shear and flexural cracks started forming or continued to propagate in the vertical cores. During the procession of sequence with the target drift of 2.07%, even more of the horizontal cores and some of the vertical cores began to shear off. Testing was terminated after cycle sequence with a magnitude of 2.89% drift. After this portion of the protocol, the interior horizontal and vertical cores had succumbed to severe shearing damage and major flexural cracks had developed around the lap splice in the external vertical cores and just below the uppermost set of vertical cores.

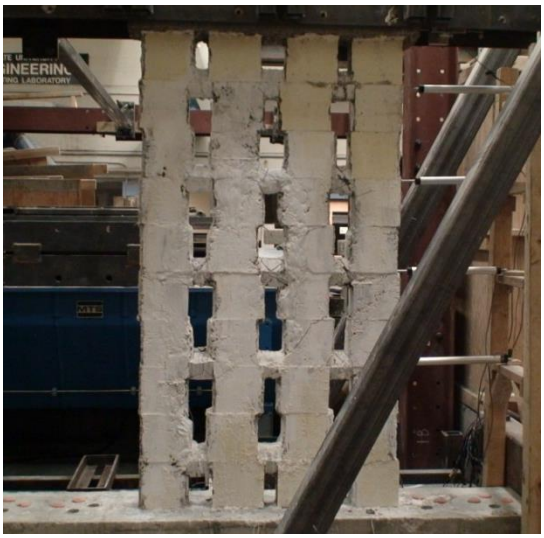

(a) 1.05% Drift

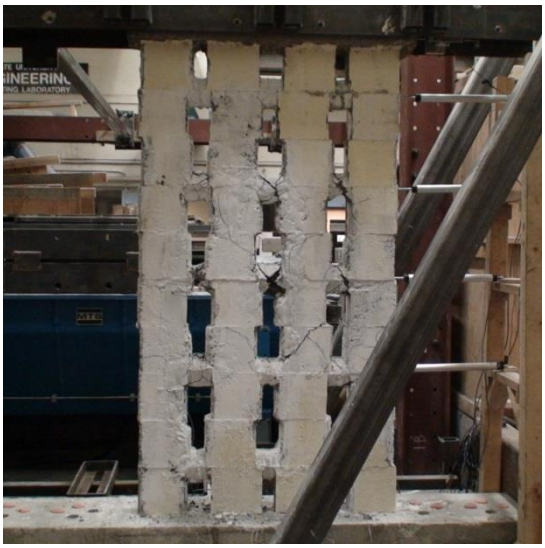

(b) 1.48% Drift

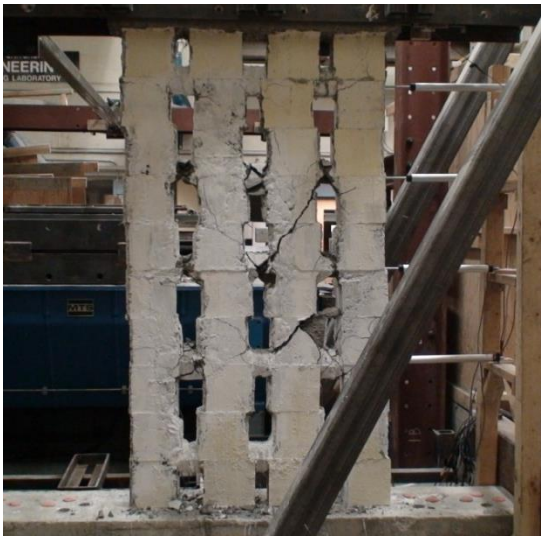

(c) 2.07% (-) Drift

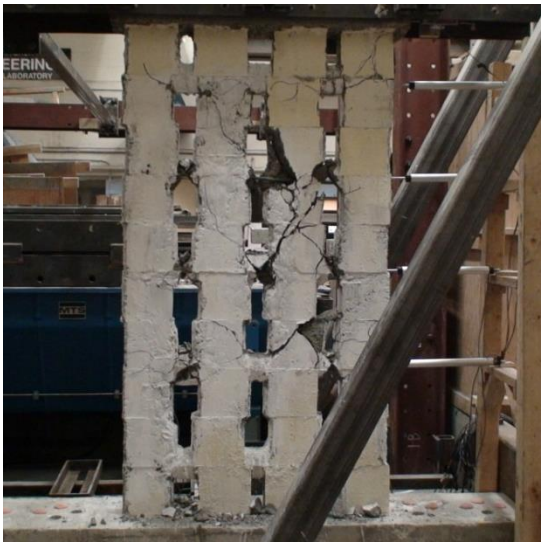

(d) 2.89% Drift

Figure 4-10: Progression to failure of specimen SWC.

4.2.2. SWS

Figure 4-11 shows the progression of damage to the baseline short wall. Specimen SWS displayed no obvious visual damage until reaching the cycle sequence for 1.05% target drift. No cracking was noticed during this sequence, but slight separation of the end

blocks, at about mid-height, was observed in both directions of load application. Some horizontal cracks were noticed in the end blocks on both sides of the wall during the 1.48% target drift sequence. Diagonal separation – which was discussed above and is clearly visible in Figure 4-11(b) – also began to occur during this phase of testing. Some faint shear cracks were also visible on the back side of the wall at about the height of the lap splice. Each of these issues continued to develop and propagate over the cycle sets for 2.07% and 2.89% drift. The peak load resistance of the wall was reached during the 2.07% drift sequence and the 2.89% sequence for the forward and reverse directions, respectively. Vertical cracks began appearing on the front side wall forms after this latter sequence. After the 3.47% drift cycles were imposed upon the wall, some of these vertical cracks had proliferated to such a degree that the wall forms were protruding from the wall. This behavior – see Figure 4-11(c) and (d) – only worsened during the last set of cycles, which had a target drift of 4.05%.

(a) 1.05% Drift

(b) 2.89% (+) Drift

(c) 3.47% Drift

(d) 4.05% Drift

Figure 4-11: Specimen SWS during and after in-plane loading protocol.

The inspection of specimen SWS showed that the horizontal cores underwent significant shear cracking and failure. The interior vertical cores showed significant shear cracking and some flexural cracking, while the external vertical cores had large flexural

cracks. Figure 4-12 shows the specimen with wall forms removed so that the internal concrete screen-grid could be examined.

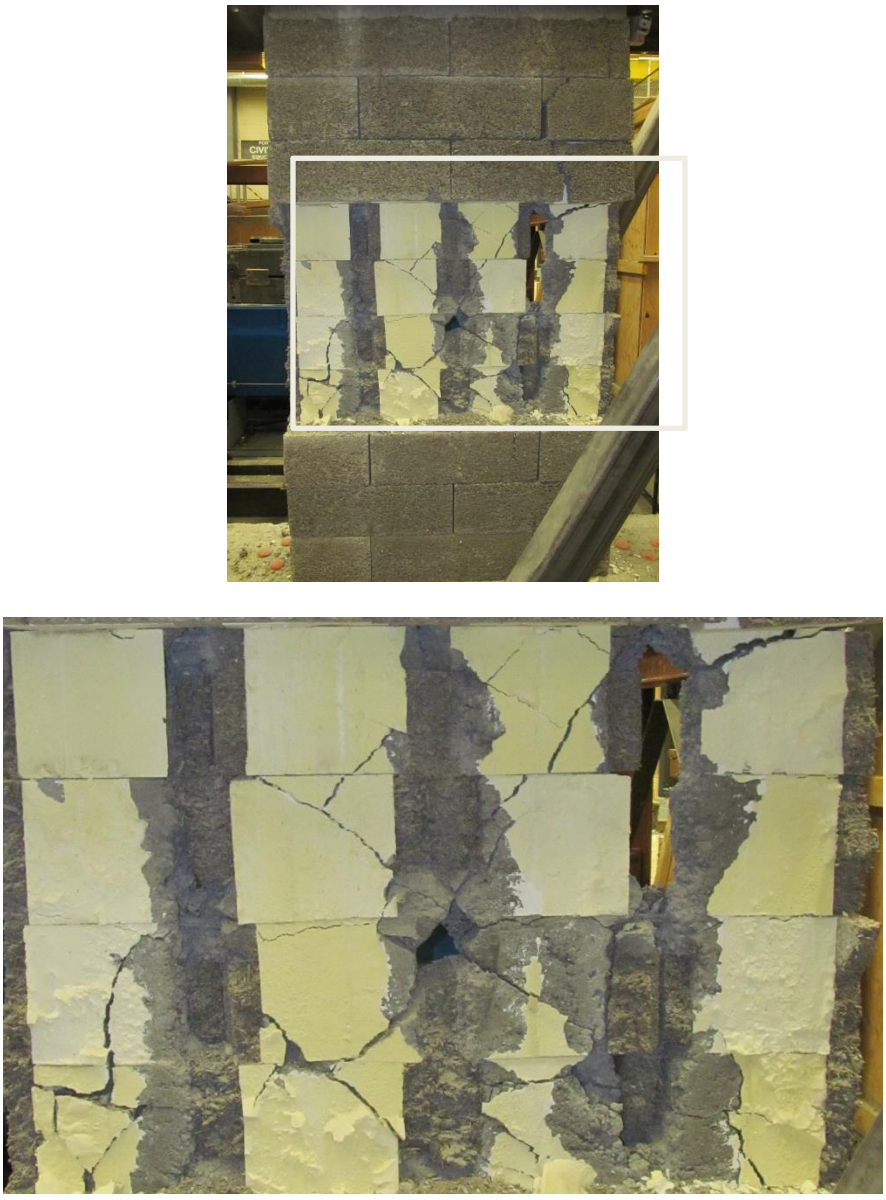

Figure 4-12: Specimen SWS with wall forms removed for inspection.

4.2.3. SWG

The short wall that was subjected to additional axial load did not display any signs of damage until the protocol reached a target drift of 1.48%, when the tension side end blocks began to separate in both directions of loading. The progression of the damage incurred by the specimen is displayed in Figure 4-13. This separation continued to increase over the next several sets of cycles, but no other damage was noticed until the target drift had reached 3.47%. At this drift, vertical and diagonal cracks began to appear in the forms on the back side of the wall. These cracks seemed to have been initiated in areas where horizontal cores were located. Some vertical cracks had also developed in the end blocks on the front side of the wall at this stage in the loading protocol. The cracking and separation only became more pronounced until the last set of cycles, when the front side of the wall forms started detaching from the wall. The target drift for this set of cycles was 5.67%.

(a) 2.07% Drift

(c) 2.89% (-) Drift

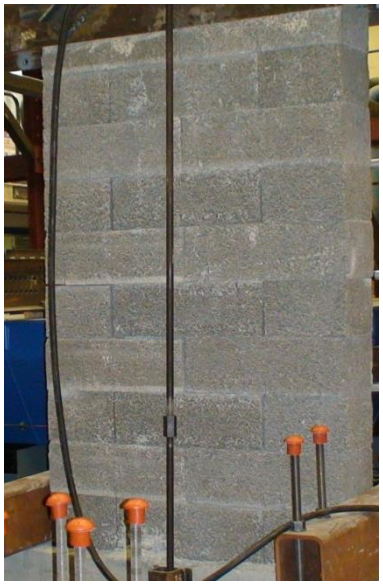

(b) 4.05% (+) Drift

(d) 5.67% (-) Drift

Figure 4-13: Progression of test on specimen SWG.

Figure 4-14 shows specimen LWG with the wall forms removed from the most critically damaged region. Upon inspection, the horizontal cores showed severe damage from shear cracking and the vertical cores displayed significant shear cracking as well.

The end blocks also had some flexural cracking around the lap splice, which was 40 in above the foundation block for this specimen.

Figure 4-14: Specimen SWG with wall forms removed for inspection.

4.2.4. Short Wall Summary

The hysteresis curves from this set of walls are shown in Figure 4-15. As was done for the long walls, the axes have the same maximums and minimums in order to facilitate comparison of the walls. Just like their longer counterparts, these walls all had significant pinching in their hysteresis curves. As could be expected, these walls demonstrated much less load resisting capabilities and initial stiffnesses than the long walls. The hystereses were also all fairly symmetric. On average, the peak resistance of the short walls was 57% lower than that of the long walls; however, the peak deformation capacity of the short walls was 20% greater than that of the long walls. The relative performance of the walls was also as expected, e.g., the wall undergoing additional axial load had higher peak load resistances and deformation capacities than the standard wall, which resisted more load and failed at higher drifts than the wall with forms removed.

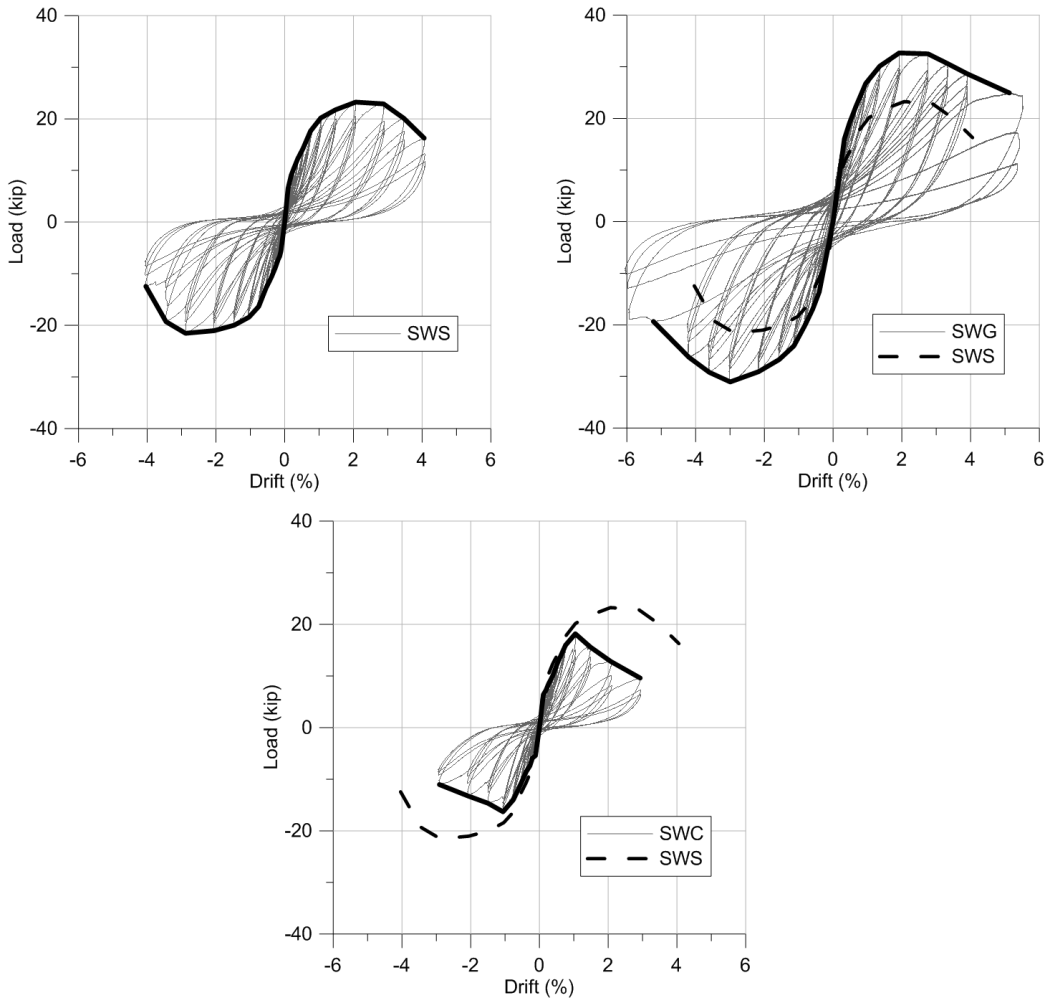

Figure 4-15: Hysteresis curves for four-foot ICF walls.

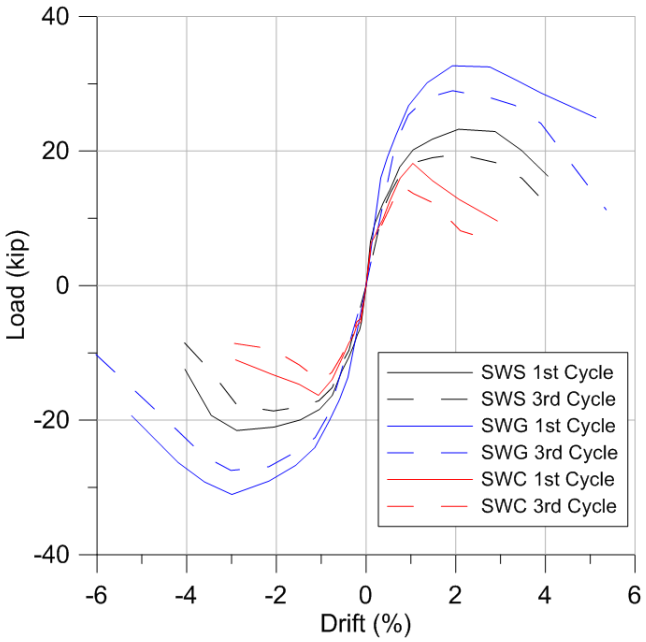

Figure 4-16: Backbone curves of 1st and 3rd cycles for short wall tests.

The backbone curves for the short walls are shown in Figure 4-16 and the peak values from each wall are shown in Table 4-2. As with the long walls, the initial stiffness values of these walls were very similar during the lower level displacement cycles, but they did not take long to diverge. The load-displacement envelopes also show that the walls with cores tended to sustain load that was close to their peak resistances over several intervals, while the wall without ICFs reached peak resistance and, during the subsequent cycle, lost a significant amount of this resistance. Also included in the table are the effective stiffness values and ductility ratios for each wall.

The average increase of load resistance in the standard wall with ICFs versus the wall without was not as pronounced for the short walls as for the long walls, but was still fairly significant at 28%. The average increase in deformation capacity between SWS and

SWC was 90%, which was also not as extreme as the increase seen in the analogous long walls.

Table 4-2: Peak load resistance and deformation capacity of each short wall.

Specimen	V_{max} (kips)		Δ_u		K_{eff} (kip/in)		μ	
	Forward	Reverse	Forward	Reverse	Forward	Reverse	Forward	Reverse
SWS	23.2	21.5	3.7%	3.6%	28.3	26.0	3.8	3.7
SWC	18.2	16.3	1.7%	2.2%	27.2	23.0	2.1	2.5
SWG	32.7	31.1	4.7%	4.4%	32.1	22.7	4.4	3.1

The axially loaded specimen saw a 41% increase in load capacity over specimen SWS, which was nearly twice the increase between LWG and LWS. At 25%, the increase in drift capacity was also more pronounced between SWG and SWS than between their longer counterparts.

4.3. **Other Performance Parameters**

In addition to the basic measures of performance reported above, a few other parameters were investigated. Two of these parameters – relative energy dissipation ratio and residual stiffness ratio – were prescribed by the same ACI reports that were used to develop the loading protocol for this procedure. Even though these reports considered reinforced concrete moment frames (ACI 2001) and unbonded post-tensioned precast walls (ACI 2008), "the recommendations in both cases followed similar patterns while dealing with reinforced concrete structural systems expected to undergo different inelastic mechanisms and exhibiting different lateral stiffness and strength characteristics between which the (SGICF) walls could potentially fit (Dusicka et al. 2011)." And, even

though these parameters were prescribed by the two ACI reports, several changes in the methods for obtaining these parameters were made in the report of Dusicka et al. (2011). Once again, for the sake of consistency, the changes made in that report will be applied for this report as well. These changes are addressed in their respective sections.

The final parameter that was examined was the deformation shape of each wall at the forward and reverse peaks of the higher level cycles. These deformation shapes were useful in determining whether walls were dominated by shear or flexure. The shapes were also useful for determining whether or not several of the assumed failure mechanisms were reasonable.

4.3.1. Energy Dissipation

Figure 4-17 shows the two parameters used for determining relative energy dissipation ratio. The amount of energy dissipated by a specimen during one cycle was defined as the area under the hysteresis curve for that cycle, A_i, which is represented by the shaded region in the figure below. An idealized hysteresis parallelogram was created for each cycle and was defined by the initial stiffness of the specimen in the forward and reverse directions, such that lines AB and CD had the same slope as the forward stiffness, K_i, and lines AE and DF had the same slope as the reverse stiffness, K'_i. The initial stiffness was taken as the slope of the line found by performing a linear regression on the load deflection curve, from zero to peak load, for each direction of loading. Lines CD and AE were drawn from the respective peak loads to the horizontal axis. Lines AB and DF were drawn from these points on the axis to horizontal lines BC and EF, respectively, which were drawn across form the corresponding peak load. The area within this

parallelogram, A_d, was defined as the idealized dissipated energy of a specimen during a single cycle. The relative energy dissipation ratio was determined by dividing A_i by A_d.

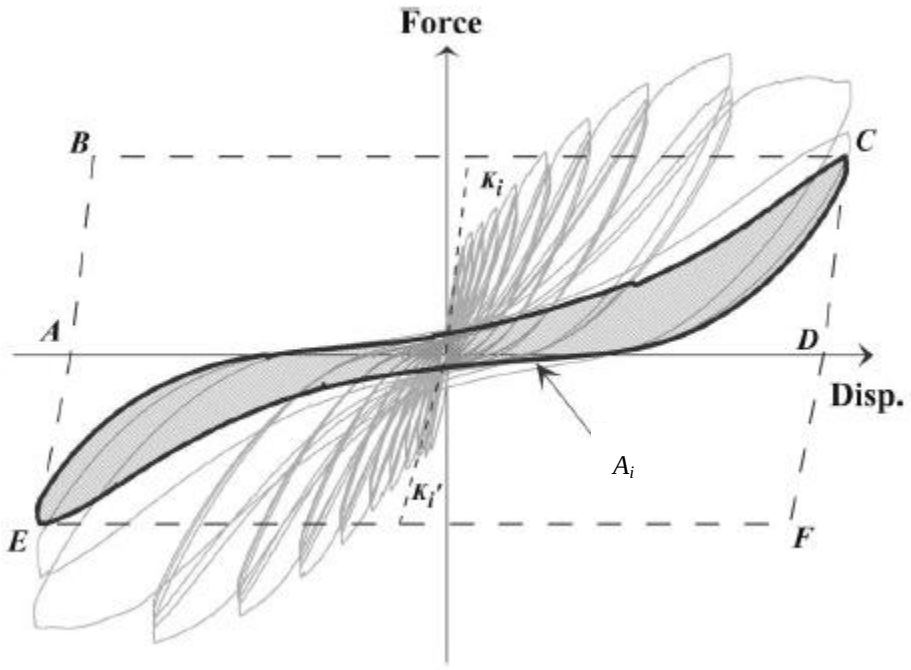

Figure 4-17: Parameters for determining relative energy dissipation ratio (Dusicka et al. 2011).

The only difference between this method for determining relative energy dissipation ratios and the method prescribed by the ACI reports (2001, 2008) was the way in which the initial stiffness values were determined. These reports define initial stiffness using the measured envelope curves in conjunction with maximum loads between 60% and 90% of the expected nominal lateral load resistance. According to ACI ITG 5.1-07, "stiffness shall be expressed as the slope for the line joining the origin of the measured response to the drift angle for the envelope at" 75% of the expected nominal load resistance (2008). Since a primary objective of this procedure was to develop a method for determining a reasonable approximation for the load resistance of an ICF wall, such a

method was not yet available when calculating the parameters prescribed by the ACI reports. Therefore, the (likely) conservative method for determining initial stiffness described above was used. The reasons that this method may have been conservative are discussed below.

Figure 4-18 shows the relative energy dissipation ratios, β, for the first and third cycles each wall specimen was subjected to. The long walls are grouped together in the top graphs and the short walls are grouped together in the bottom graphs. Each graph also features a dashed horizontal line at the value of 0.125. In order to satisfy the criteria set out by the ACI reports used to develop the load protocol (ACI 2001, 2008), β should not be less than 0.125 for the third cycle of any target drift equal to or greater than:

$$0.9 \leq 0.8\left(\frac{h_w}{l_w}\right) + 0.5 \leq 3.0 \qquad \text{(ACI ITG-5.1 Eq. 5.1)}$$

where:

$\frac{h_w}{l_w}$ = a wall's aspect ratio.

With the exception of LWC, all walls satisfied this criterion. However, the only walls that did not have relative energy dissipation ratios that dropped below 0.125 at any target drift were specimens LWG and SWG.

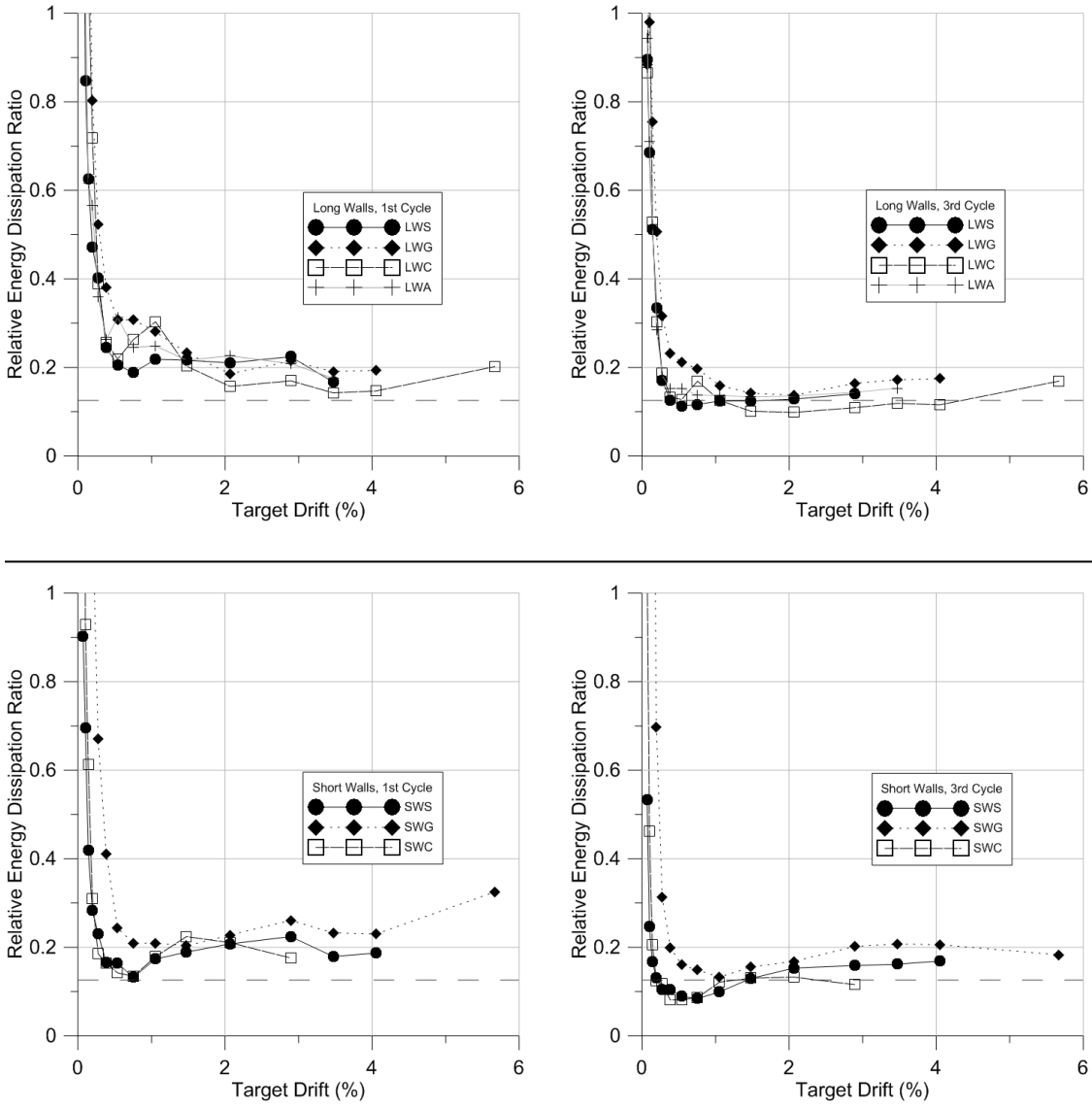

Figure 4-18: Relative energy dissipation ratio for each set of walls.

4.3.2. Residual Stiffness

Figure 4-19 shows the values used to determine residual stiffness ratio. Initial stiffness for each direction was obtained using the same method that was used for calculating the energy dissipation ratio. For each set of cycles, the residual stiffness was determined by performing a linear regression on the (load-deflection) data between 10% of the limiting drifts for both the forward and reverse portions of the cycle. The limiting

drifts were defined as the drifts corresponding to the points in each half-cycle when peak load resistance occurred. For each case, the stiffness was taken as the slope of the regressed line. This method for determining residual stiffness was in line with the method used by Dusicka et al. (2011), but differed from the ACI reports in that these reports required using secant stiffness between the ranges of ± 10% of the limiting drifts. The residual stiffness ratio was taken by dividing the residual stiffness by the initial stiffness.

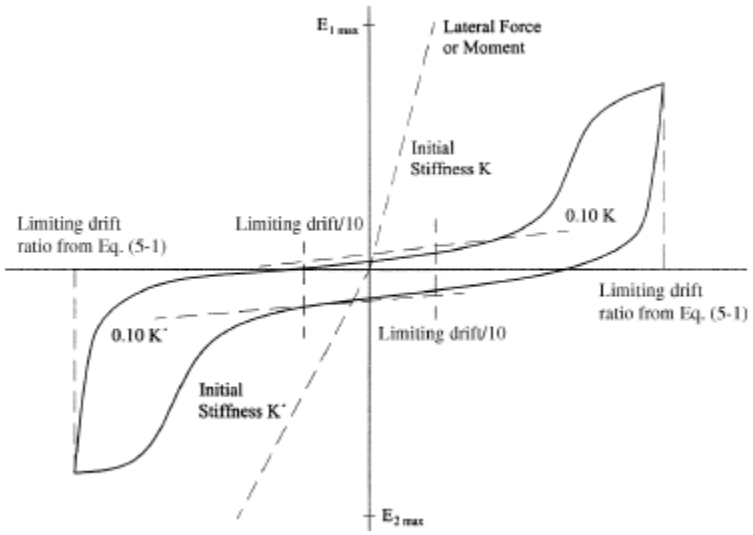

Figure 4-19: Hysteretic behavior disapproved of by ACI ITG-5.1-07. Image from ACI (2008).

The relative stiffness ratios for the third cycle of each test at each drift are shown in Figure 4-20. The ACI reports specify that on the third iteration of each cycle, the residual stiffness ratio should be either 0.05 (for moment frames with drifts up to 3.5 %, 2001) or 0.1 (precast shear walls with drifts up to 3.0%, 2008). For a frame of reference, two horizontal dashed lines have been inserted into each graph at ratios of 0.05 and 0.1.

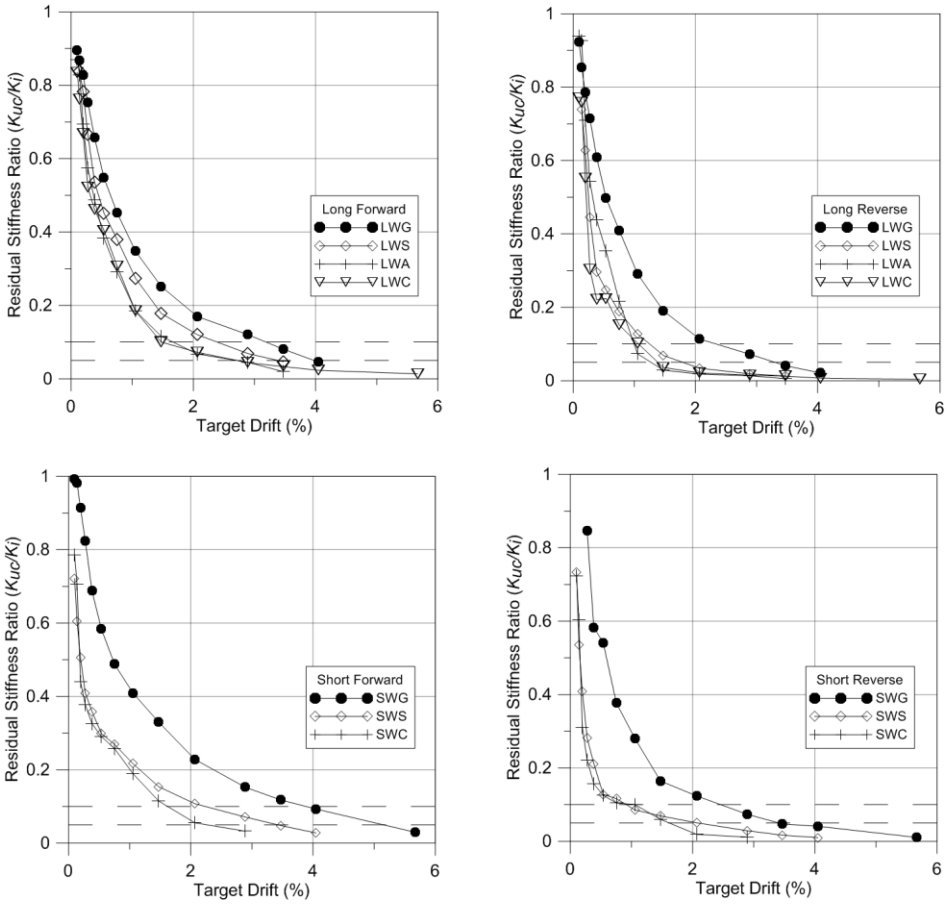

Figure 4-20: Relative stiffness ratios for the third cycle of each test.

There are several important observations to be made from examining Figure 4-20. First, the stiffness of each wall degraded more rapidly in the reverse direction than in the forward direction. A possible cause for this phenomenon could be that loading in the forward direction had some initial loss of stiffness in the reverse direction before the reversal of the cycle commenced. More importantly, no wall satisfied either criterion (for moment frames or precast walls) set forth by the ACI reports.

4.3.3. Wall Deformation Shapes

The wall deformation shape for each long wall is shown in Figure 4-21. The legend to the right of each graph shows the magnitude and direction of the target drift.

For instance, 1.05F refers to the forward portion of the cycle with a target drift of 1.05% and 1.05R refers to the reverse portion of that cycle. The markers indicate the different heights at which displacement was measured, i.e., the location of each LVDT. The axis labeled “Height” shows the height from the bottom of the wall/top of the foundation block. The drifts were taken during the first iteration of each set of cycles.

On the surface, these graphs show that, with the exception of specimen LWA, the long walls behaved similarly. However, in order to contextualize these graphs, the failure modes of each wall should also be considered.

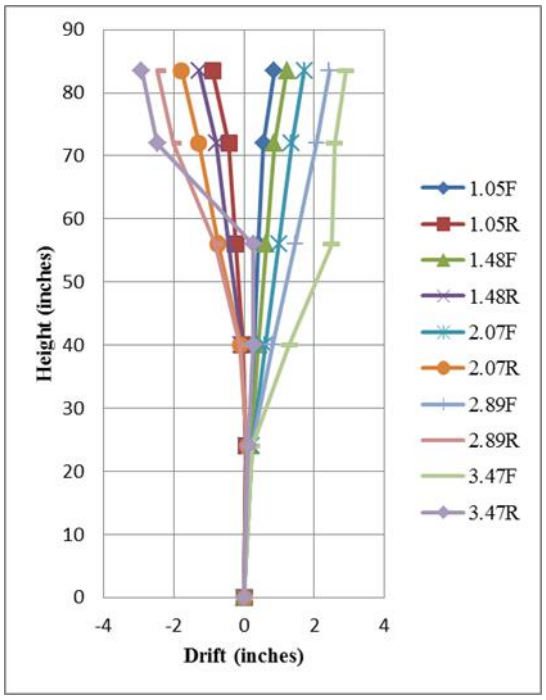

(a) LWS

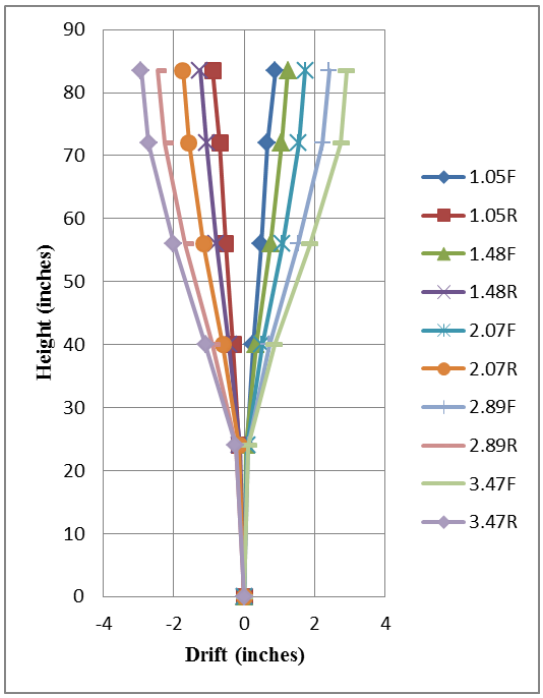

(b) LWC

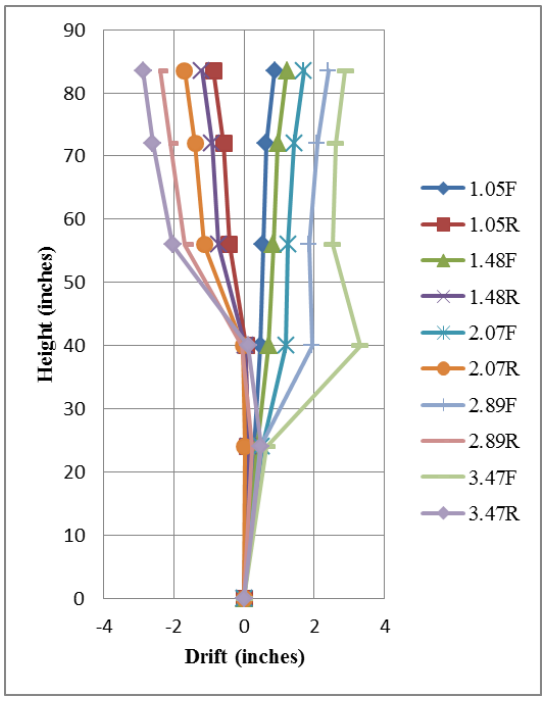

(c) LWA

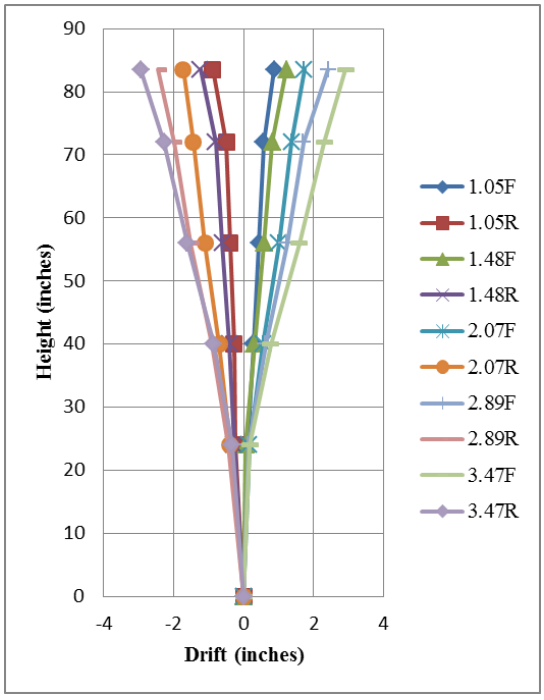

(d) LWG

Figure 4-21: Deformation shapes for the long walls.

Specimen LWC started developing flexural cracks around the lap splice (30 in) during the cycle sequence with a target drift of 1.48%. Figure 4-21(b) shows that after this sequence, hinging at that level (or between the LVDTs that were located at 24 in and 40 in) became quite pronounced. Specimen LWS started acting in a similar manner at the same target drift, but only in the forward direction. Figure 4-21(a) shows that, in the reverse direction, specimen LWS underwent hinging at about 40 in, which was consistent with the flexural cracks discovered at that height in the reinforced concrete cores after testing had been terminated. Specimen LWA actually performed in a similar manner to LWS in that hinging occurred at two different heights, depending on the direction of loading. Flexural cracks had actually occurred below and above the fifth end block, or at about 32 in and 40 in, on the right side of the wall, which was the tension side during reversed loading. The propagation of these cracks in conjunction with reversing the cycle so that this core was in compression caused this portion of the wall to dislocate. This phenomenon explains why Figure 4-21(c) looks so skewed for the cycle with a target drift of 3.47%.

The real anomaly of this set was specimen LWG. From Figure 4-21(d), this wall appears to hinge in the later cycles, but no flexural cracking was observed after testing had been terminated. The spliced reinforcement could have provided some extra stiffness to the lower cores, or the addition of the axial load could have caused the other failure mechanisms to occur before true hinging took place.

Figure 4-22 shows the deformation shapes of the short walls during the higher level cycles. One important note about the figure: for specimen SWS, the LVDT stand

was not properly ballasted and the stand moved with the wall when the wall was being pushed, i.e., during the forward portion of each cycle. Because of the slow rate of loading, this movement was not noticed until well after the test had been completed. The stand would move back when the wall was centered and would not budge during reverse loading; however, there is no guarantee that the stand returned to the same initial position after each stage of forward loading. Despite this fact, the wall's deformation shape in the reverse direction seems congruent with the wall's mode of failure, which was described above.

Because of the reasons listed above, Figure 4-22(a) may not be entirely reliable. However, by considering the modes of failure in conjunction with the wall deformation in the reverse direction, the graph may still have some merit. As was shown for the long wall specimens, large flexural cracks in the vertical cores of the walls corresponded to hinging behavior in the area of those cracks. Large flexural cracks were observed in specimen SWS along the lap splice, and Figure 4-22(a) shows that hinging did occur, at least in the reverse direction. While Figure 4-11(b) shows that hinging likely occurred in the forward direction, note the separation of the end blocks in the region of the lap splice, this behavior cannot entirely be confirmed by the measured wall deformation shape because of the movement of the LVDT stand.

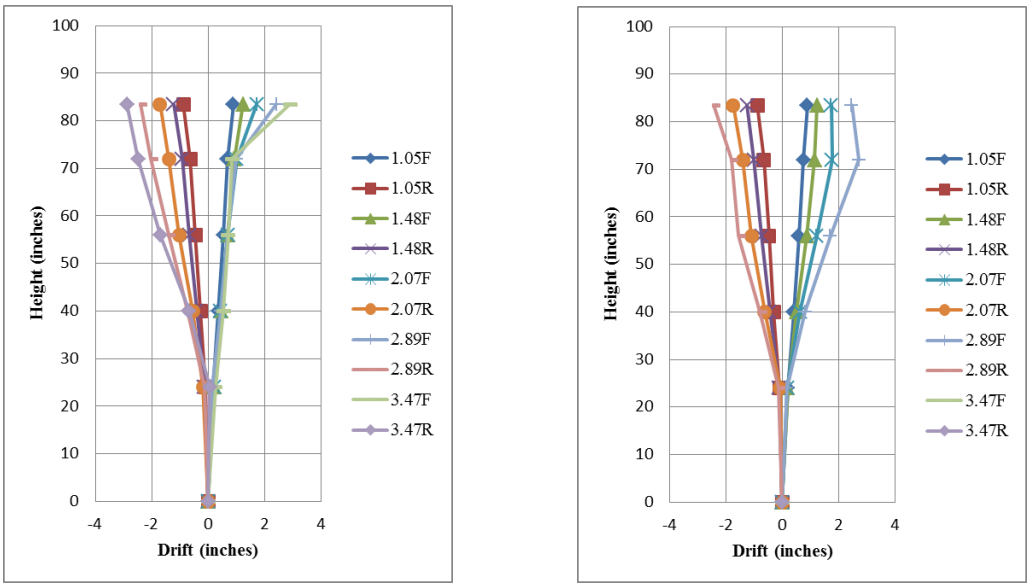

(a) SWS (b) SWC

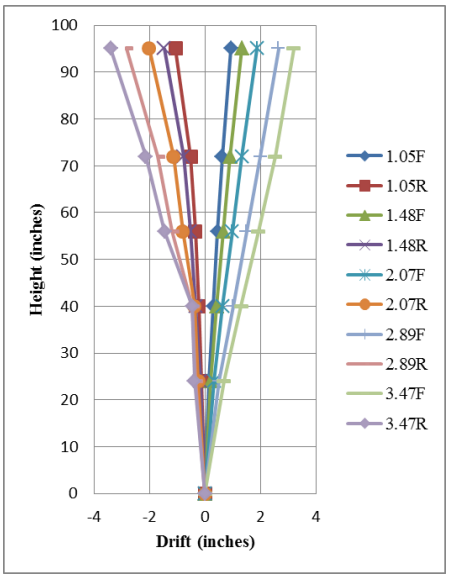

(c) SWG

Figure 4-22: Deformation shapes of short walls.

Figure 4-22(b) shows what was earlier assumed: that hinging around the lap splice in specimen SWC became pronounced during the cycles with 1.48% target drifts. Figure 4-22(c) shows that specimen SWG behaved similarly to specimen LWG in that the wall did not show any serious hinging effects until even higher level cycles (relative to the

other walls with similar aspect ratios). Unlike specimen LWG, SWG did show pronounced hinging in these later cycles, albeit in the reverse direction only, and flexural cracking was observed (after the test) in the region of the lap splice.

With the exception of specimen LWG, all walls had similar deformation patterns. During the lower level cycles, the deformation behavior of the walls was shear-dominated, i.e., the deformed wall shape resembled a rhombus. This behavior continued until the middle three rows – the top and bottom rows experienced considerably less damage then the rest – of horizontal cores had undergone shear cracking to a degree that they were transferring little to no load. This phenomenon was quickly followed by the development of flexural cracks around the lap splice. As the target drifts were increased, these cracks continued to propagate and, as the cracks continued to propagate, the hinging behavior of the wall became more pronounced. This hinging was a flexure-dominated behavior, but the portion of the wall above (or, in the cases of LWC and SWC, between) the hinges still maintained a rhomboid shape when deflected. At least, until the walls became so damaged that the anchors to the LVDTs loosened or dislodged. Considering this behavior, the walls could be said to have exhibited both flexure and shear-dominated deformation at failure. Specimen LWG was different because it exhibited this combined deformation in the forward direction but only shear-dominated deformation in the reverse direction at failure.

Chapter 5: COMPARISON OF TEST RESULTS

In order to develop a reasonable basis for design for the Faswall screen-grid ICF walls, prudence dictated that the results obtained from this procedure be compared to other theoretical and experimental values obtained for similar wall types. These comparisons were mainly confined to the load resistance capabilities of the walls, but some consideration was made for drift capacities, energy dissipation ratios, and residual stiffness values.

5.1. Previous ICF Tests

5.1.1. Faswall Components (Werner)

The investigation conducted for Werner's thesis ultimately showed that the presence of the Faswall ICF material increased the maximum load resistance of the specimen by 45-150%. Because of the premature failure that occurred in the supports, however, there was no way to quantify the effect that the forms had on the drift capacity of the components. For the sake of comparison, the increase in peak load resistance for the APEX samples was 25-50%., with no appreciable increase in drift capacity.

The differences in peak load resistance between specimens with and without forms were not as pronounced for this procedure, but were still significant. The walls with forms saw increases in peak shear of 28% and 56% for short walls and long walls, respectively. The contribution of the forms to drift capacity of the specimens was even more significant, with increases of 90% and 114% for the high and low aspect ratios, respectively.

While the component tests conducted by Werner indicated that the performance of the walls would be significantly improved by leaving the forms, the results simultaneously overshot the forms' contribution to load resistance while not providing much insight into how drift capacity would be affected.

5.1.2. APEX Walls (Dusicka et al.) and Reinforced Concrete Walls (Kay et al.)

The walls tested by Dusicka and Kay, as mentioned previously, were part of the same testing sequence and, as such, will be considered together in this section. The reinforced concrete walls discussed in Kay et al. were meant to act as benchmarks for direct comparison to the APEX walls. The concrete walls were designed using an equivalent thickness that was prescribed by the equation for maximum shear strength in ICC-ES ESR 1770 (2012). This is the evaluation report used to design APEX systems. The shear equation in this report, which will be discussed at greater length later, treats an APEX wall as a reinforced concrete wall with equivalent thicknesses and lengths. From this equation, the equivalent thickness of the reinforced concrete wall was equal to 75% of the diameter of the concrete cores in the APEX forms. Since the diameter of these cores was 6 in, the equivalent thickness of the benchmark wall was 4.5 in.

From Kay et al., the experimentally observed shear capacity of the 0.89:1 aspect ratio walls under only self-weight was, on average, 28% lower than the results obtained using the ICC-ES equivalent shear equations. The results for the same walls under additional gravity loading were, on average, 9.8% lower than the theoretical values, which did not consider the influence of axial load. The reinforced concrete walls were

only tested under self-weight and difference between the experimental and theoretical values ranged from -17% to 20%, for an average of about 3%. The reinforced concrete walls, which were not axially loaded, had shear resistances that, on average, were 82% higher than the APEX wall under self-weight and 43% greater than the APEX wall under additional gravity loading. Again, these values were for the 0.89:1 aspect ratio walls.

The APEX walls with aspect ratios of 0.89:1 and that were not subjected to additional gravity loading had a shear capacity that was, on average, 23% lower than specimen LWS (the standard Faswall wall with an aspect ratio of 0.87:1). The 0.89:1 APEX wall that was subjected to the 10 klf gravity loading had a shear capacity that was 17% less than specimen LWG, on average. The shear capacity of the reinforced concrete walls was 40% and 18% greater than specimens LWS and LWG, respectively.

The purpose of these specific comparisons was to show that there may be some use in using the same theoretical shear equation (as prescribed by the ICC-ES) for both APEX walls and Faswall walls. Given the relative shear capacities reported above, this presumption seemed valid and is investigated later on in this chapter. This comparison only looked at similar aspect ratios in an effort to minimize the variables considered; however, the investigation into the efficacy of using the ICC-ES APEX shear equation will consider all of the Faswall walls tested.

In addition to peak strength, there were several other parameters to compare between the different sets of tests. In addition to peak strength and drift capacity, Dusicka et al. also reported the energy dissipation ratios, residual stiffness values, and idealized ductility ratios for each APEX wall.

Similar to this study, the energy dissipation ratios of the APEX walls approached 0.1 at about 0.5% drift on the third cycle, and mostly maintained that ratio for the third cycles of the remaining target drifts. However, the ACI reports (2001, 2008) specify that this ratio should not drop below 1/8. The majority of the pertinent Faswall walls stayed above (or around, in the case of LWS) this number but, as stated above, the stiffness value used to determine the idealized energy dissipation of each cycle was likely conservative. Dusicka et al. used the same metric for determining this initial stiffness, so changing this metric could positively affect both wall sets. The reason this initial stiffness values for each tests' wall sets may have been conservative was that these values were obtained for using load-displacement data for the very first cycle, which should be when the system is stiffest. The ACI reports specify using a secant value that occurs at a displacement corresponding to about 75% of the estimated peak load resistance of the system. This secant value must inherently be lower than the stiffness of the initial cycle because of the certain degradation the system will undergo throughout subsequent cycles. For the Faswall walls, there are currently no equations accepted for determining a reasonable peak capacity, so determining a stiffness based on that value was not possible. If such an equation were to be accepted, there may be some merit in determining the effective stiffness of the system using that equation. Kay et al. also calculated the energy dissipation ratio for the reinforced concrete walls, but the report does not indicate whether the method used was the same as the ICF walls or the method prescribed by Hawkins et al., which corresponds to the ACI reports. Kay's report states that energy dissipation was calculated as specified by Hawkins et al. for all walls, but, as stated

above, this would not be possible for the ICF walls. Either way, the benchmark walls easily satisfied this criterion by dropping to and maintaining an energy dissipation ratio of about 0.2 during the third cycles.

Using the initial stiffness value as discussed above also may be conservative for determining residual stiffness ratios for ICF walls. While Dusicka et al. did not calculate the residual stiffness ratios, simple residual stiffness was considered. Since all of the long APEX walls failed at drifts below about 2.5%, the horizontal axes for residual stiffness were capped at 2.25%. The graphs show the same behavior as the Faswall graphs, where the majority of a wall's stiffness was lost prior to 1% drift. Unfortunately, since the values for residual stiffness were not reported as ratios, comparing these values to the accepted values of the ACI reports would be both tedious and imprecise and so no direct comparison is to be made. This is dually unfortunate as using the initial stiffness as the denominator seems conservative when compared to the method prescribed by the ACI reports, which, just like determining the energy dissipation ratios, call for determining secant stiffness values based on the presumed strength of the walls.

5.1.3. SGICFs Tested at UCI (Yland)

Yland's dissertation investigated several parameters of performance for ICFs, but most pertinent to this study was the observation of ICF walls under in-plane cyclic loading. As was mentioned in the Literature Review section (1.2.3), the walls tested by Yland failed at about 1% drift, which was considerably lower than the APEX (2.5% drift, on average) and Faswall walls (3.6% drift, on average) with forms left in place. Werner suggested that this low drift capacity, relative to the APEX walls, could have been

influenced by either concrete strength or core spacing, both of which were lower than the respective values for the APEX walls. While both of these factors seem reasonable, another considerable factor exists: the testing schedule. As mentioned in the Literature Review section cited above, Yland's walls underwent 57 fully-reversed cycles before getting to a target drift of 1%, while the specimens tested at PSU (e.g., APEX walls, Faswall walls, and APEX and Faswall components) only underwent 25 fully-reversed cycles before reaching a target drift of 1%. As was previously stated, the walls and components tested at PSU were subjected to a loading protocol that followed the prescriptions of two ACI reports (2001, 2008). One major admonition made by each report was "(i)f steps are too small, the system may be unrealistically softened by loading repetitions (ACI 2008)." Although this provision goes on to say that steps that are too small can lead to artificially low peak load resistances and artificially high drift capacities, there may be a point where the steps are so small that the degradation of the wall affects both load resistance and drift capacity.

For the 1:1 aspect ratio, Yland's upper-bound wall (in which reinforcing was centered and tied) reached a peak load of about 79.6 kips. This value is 7.1% higher than the average peak load of specimen LWG (Yland's walls were subjected to gravity loading of 10 klf as well).

5.2. **Faswall Shearwall Design Considering only the Reinforced Concrete Cores**

Current practice dictates that any design for shear walls constructed with Faswall ICF forms must consider only the reinforced concrete cores when considering in-plane lateral load resistance. In order to simplify this process, ShelterWorks commissioned a

structural engineering firm (AE Group, based in Eugene, OR) to develop load tables. The table intended for use in shear wall design considered only the length of the wall, so long as other criteria were met. These criteria included, but were not limited to: 5-in-thick cores; #4 reinforcing, Grade 60; vertical reinforcing was 12-in on center; horizontal reinforcing was 16-in on center; 2500 psi concrete at 28 days; nominal maximum aggregate size of 3/8in; and slump between 6 in and 7 in. The story height was not to exceed 10 ft, with total wall height limited to 30 ft. Unfortunately, for the purposes of this paper, the calculations used to develop this table were not available.

From these tables, a 4-ft wall was given a capacity of 766 plf, and an 8-ft wall was given a capacity (by linear interpolation) of about 1,139 plf. This capacity had to be interpolated because no value was given for wall lengths between 80in and 116in. Therefore, the capacities of the walls, obtained from these tables, are 3.06 kips for 4-ft walls and 9.11 kips for 8-ft walls.

Another method for considering the in-plane shear resistance of the walls was using the ACI equation for minimum shear strength of concrete. Several assumptions were made in utilizing this equation. The first assumption was to ignore the axial loads, both self-weight and any additional gravity loading, to which the wall may have been subjected. The second assumption was that the cores acted together as a single wall. To illustrate: an 8-ft wall had eight cores, and each core was assumed to be 8 in long. The resulting "equivalent" wall then would be 64 in in length (or eight times 8 in). This assumption ignored the contribution of the horizontal cores, as well as any contributions

from the steel and wall forms. The shear strength was given by the following equation from ACI 318-11:

$$V_c = 2\lambda\sqrt{f'_c}b_w d \qquad \text{(ACI 11-3)}$$

where:

$\lambda = 1.0$ for normal-weight concrete

b_w = Wall thickness (5 in)

$d = 0.8l$

l = Equivalent wall length (64 in or 32 in, depending on aspect ratio)

Each wall's individual average value for f'_c (in psi) was used in this equation. Table 5-1 compares the experimentally obtained average shear resistance of each wall to the theoretically determined values which were obtained using the procedures previously discussed. No strength reduction factors were applied to any of the theoretical values in order to best approximate capacity. This equation will henceforth be known as the modified ACI shear equation, because of the assumption that the vertical cores form a single wall. The load table values (which assume a concrete compressive strength of 2500 psi) were not altered to consider the f'_c of each wall.

Table 5-1: Comparison of peak experimental load resistance to theoretical ACI and load table values.

Wall Designation	Experimental	ACI		Load Table	
	V_{max} (kips)	V_c (kips)	V_{max}/V_c	E (kips)	V_{max}/E
LWS	61.7	37.8	1.6	9.1	6.8
LWA	43.4	37.8	1.1	9.1	4.8
LWC	39.3	40.2	1.0	9.1	4.3
LWG	73.1	38.5	1.9	9.1	8.0
SWS	22.4	20.5	1.1	3.1	7.2
SWC	17.3	19.9	0.9	3.1	5.6
SWG	31.9	16.3	2.0	3.1	10.3

On average, the experimental shear resistances were 6.7 times greater than the theoretical values obtained from using the load tables. These approximations were extremely conservative, even for the walls with no forms or increased spacing of vertical reinforcement. The ACI equation yielded more reasonable approximations. The results were still fairly conservative for the walls with forms – the experimental values were 1.4 times greater than the theoretically obtained values; and this percentage would only increase with the use of a strength reduction factor. The theoretical ACI values were unconservative for the core-only walls; the experimental walls reached peak loads that, on average, were about 92% of the values estimated by the ACI equation. Because of the slim likelihood that core-only walls would actually be used in any structural application, both of these methods may be too conservative.

5.3. **Wall Design Using ICC ESR 1770 Equations**

The International Code Council Evaluation Service (ICC-ES) released a report (ICC-ES 2012) outlining the use of Apex ICF systems in order to comply with the 2009 *International Building Code* (IBC) and the 1997 *Uniform Building Code* (UBC). Within this report there a couple of equations provided to determine the shear strength of components built using the Apex system. The equation used by Kay et al. in an effort to predict the lateral load resistance of the Apex and benchmark walls was:

$$V_c = 2\varphi\psi b_{eq} d\sqrt{f'_c} \qquad \text{(ICC-ES Equation 4.1.1.7)}$$

where:

φ = Strength reduction factor based on pertinent codes.

ψ = Grid-factor of 0.85.

b_{eq} = Width of an equivalent rectangle section (4.5 in).

d = 0.8l.

l = Length of the wall (in).

f'_c = Compressive strength of concrete (psi).

The equation proved to overestimate the strength of the APEX walls, but there may be a simple explanation for this: the equation was meant for "members subject to shear and flexure, such as lintels (ICC-ES 2012)." While this definition does not directly exclude walls, the definition for the next design equation in the report specifies use for "(i)n-plane racking shear strength of shear walls (2012)." The value yielded by this equation is about 78% of the value obtained from the previous equation, which would have been more representative of the performance of the APEX walls. Also worth noting, the strength reduction factor used by Kay et al. was 1.0. Using the standard ACI shear reduction factor of 0.75 would have yielded theoretical results that were closer to the experimental results.

Both of these equations were considered for the Faswall walls, but the equation for V_c proved to be more representative of the experimental values. The other equation was more conservative than the modified ACI equation used above. Table 2-1 compares the average peak load resistance of each Faswall wall to the theoretical values obtained using the equation for V_c. The theoretical values are shown with (φV_c) and without a shear strength reduction factor of 0.75, as prescribed by ACI. The value for b_{eq} was

chosen to be the actual width of the vertical concrete cores (5.5 in) since the cores were already rectangular. As with the ACI shear equation above, each wall's average f'_c was used to calculate respective values of V_c.

Table 5-2: Comparison of experimental peak loads and theoretical peak loads based on ICC-ES equation.

Wall Designation	V_{max} (kips)	V_c (kips)	V_{max}/V_c	φV_c (kips)	$V_{max}/\varphi V_c$
LWS	61.7	48.3	1.3	36.2	1.7
LWA	43.3	48.3	0.9	36.2	1.2
LWC	39.3	51.2	0.8	38.4	1.0
LWG	73.1	49.1	1.5	36.8	2.0
SWS	22.4	26.2	0.9	19.6	1.1
SWC	17.2	25.3	0.7	19.0	0.9
SWG	31.9	20.7	1.5	15.6	2.0

On average, the experimental values were 1.1 times greater than the values obtained for V_c and 1.4 times greater than the values obtained for φV_c. The experimental values were about 83%, on average of the values of V_c for walls LWA, LWC, SWS, and SWC; but the experimental values were 1.4 times greater for specimens LWS, LWG, and SWG. The reason for examining a theoretical value with and without a strength reduction factor was specimen LWA. The unfactored theoretical load was 12% higher than the experimental value, but the factored load was 16% lower. While the values for the unfactored equation may be conservative for LWS, LWG, and SWG, specimen LWA represents the standard in above grade residential construction for these walls.

Chapter 6: CONCLUSIONS

There were several objectives that this study set out to accomplish, but, during the course of investigation, several new questions arose as well. The primary objective was to observe the behavior of walls built with the Faswall ICF system under in-plane cyclic loading. Several other objectives fell directly under this rubric: what were the effects of the wall forms, gravity loading, and altered reinforcement had (independently) on a wall's performance; how these walls performed compared to other ICF walls and components; how these walls performed compared to some theoretically obtained values of shear resistance; and how to determine a reasonable method for approximating the shear capacity for walls built with Faswall wall forms.

6.1. **Wall Performance**

On average, the presence of the wall forms increased the shear strength of the walls (considering the same gravity loading and reinforcing detail) by 28% and 56% for walls with high and low aspect ratios, respectively. These forms also increased the drift capacity of these same walls by 90% and 114%, on average. The forms also increased the idealized ductility ratio of these walls by between 59% (for high aspect ratios) and 76% (for low aspect ratios).

By observing the contribution of the wall forms, some determinations could be made about the common design practice of ignoring the forms altogether when considering the lateral load capacity of a wall. The material tests performed by Werner and Yland show that at strains of up to 0.3%, at which concrete would be expected to

yield, the resistance of ICF material was practically negligible compared to that of concrete. Yet the material tests performed by Yland, the component tests performed by Werner, and the full-scale tests performed by Dusicka and Kay, as well as those performed in this procedure, show that both EPS and wood-based ICF material made significant contributions to the strength and deformation capacities of ICF walls.

The addition of a 10 klf axial load also made significant contributions to the performance of the Faswall ICF walls. The long walls (low aspect ratio) saw a 21% strength increase, while the short walls (high aspect ratio) saw a 42% strength increase with the addition of axial load. The additional load also increased the drift capacities of the long and short walls by 13% and 25%, respectively. These tests show that any theoretical design equation that excludes gravity load would most likely be conservative.

6.2. **Recommendations for Design**

Considering the comparisons made in Chapter 5:, the best approximation for theoretical design of shear strength of walls comprised of Faswall wall forms appears to be the ICC-ES equation for E_{nt} (V_c). The equation may be somewhat conservative for walls with reinforcing in each vertical core, and even more so if gravity loading is to be considered. However, for above-grade walls with reinforcing at 24 in on center, the application of a load factor may be necessary. The inclusion of a load reduction factor may not be problematic for the other wall types, because, even if the theoretical values yielded were conservative, they would still be within an order of magnitude of the actual capacity of the wall, unlike the values obtained by using the simplified Faswall load table.

The modified ACI shear equation (discussed in Section 5.2) ended up being more conservative than the ICC-ES equation, but would still present a better alternative to the simplified load tables. The use of a load factor less than 1.0 would likely not be necessary as all wall with forms had experimental shear values that were considerably higher than the theoretical values. Specimen SWS had the smallest difference at 9.1%.

REFERENCES

American Concrete Institute. *Acceptance Criteria for Moment Frames Based on Structural Testing.* Farmington Hills, MI: ACI T1.101, 2001.

—. *Acceptance Criteria for Special Unbonded Post-Tensioned Precast Structural Walls Based on Validation Testing and Commentary.* Farmington Hills, MI: ACI ITG-5.1-07, 2008.

—. *Building Code Requirements for Structural Concrete (ACI 318-11).* Farmington Hills, MI: American Concrete Institute, 2011.

American Society for Testing and Materials. *ASTM C143/C143M - 12.* West Conshohocken, Pennsylvania: American Society for Testing and Materials, 2012.

—. *ASTM E 2126-08 Standard Test Methods for Cyclic (Reversed) Load Test for Shear Resistance of Vertical Elements of the Lateral force Resisting Systems for Buildings.* West Conshohocken, Pennsylvania: American Society for Testing and Materials, 2008.

Dusicka, P., and Kay, T. "In-Plane Lateral Cyclic Behavior of Insulated Concrete Form Grid Walls." *Journal of Structural Engineering* (American Society of Civil Engineers), 2011: 1075-1084.

Gajda, J., and Dowell, A.M. *Concrete Consolidation and the Potential for Voids in ICF Walls. Skokie, IL: Portland Cement Association, 2003.*

Hawkins, N.M., and Ghosh, S.K. "Acceptance Criteria for Special Precast Concrete Structural Walls Based on Validation Testing." *PCI Journal*, 2004: 78-92.

ICC Evaluation Service. *ICC-ES Evaluation Report ESR-1770: APEX Block Interlocking System.* Report, ICC-ES, 2012.

Kay, T., and Dusicka, P. *Reversed Cyclic Deformation Tests on Insulated Concrete Form Walls Using the APEX Blocks Interlocking System.* Report, Portland, OR: Portland State University, 2009.

National Association of Home Builders. *In-Plane Shear Resistance of Insulating Concrete Form Walls.* Upper Marlboro, MD: NAHB Research Center, 2001.

Raynor, D. J., Lehman, D. E., and Stanton, J. F. "Bond-Slip Response of Reinforcing Bars Grouted in Ducts." *ACI Structural Journal*, 2002: 568-576.

ShelterWorks, LTD. *Faswall Technical Installation Manual.* Philomath, OR: ShelterWorks, 2010.

Werner, C.S. *Cyclic Behavior of Screen Grid Insulated Concrete Form Components.* Portland, OR: Portland State University, 2010.

Yland, C.V. *Experimental and Analytical Studies of the Structural Performance of Innovative Structural Grid Walls.* Irvine, California: University of California Irvine, 2000.

APPENDIX: CONCRETE MIX DESIGN

Ross Island Sand & Gravel Co.
3011K-70/30 KURTZ MIX [0]
Strength Compressive: 3000 psi
03/18/2013

Compressive Strength :	3000 psi at 28 days	Source of Concrete : Ross Island Sand & Gravel Co.	
Aggregate size :	3/8" -- 9.5 mm	Construction type : BLOCK FILL	
Air :	3.0 ± 1.5 %	Placement : CHUTE OR PUMP	
Water/Cement ratio :	0.543	Unit Weight : 147.26 pcf	
Slump :	5.00 to 8.00 in	Design Date : 06/29/2010	

Constituents :	Quantity	Density	Volume
Type I/II Cement (Cement)	489 lb	3.150	2.49
ASTM C989 Grade 100 Slag (Cement)	122 lb	2.890	0.68
Water	330 lb	1.000	5.29
ASTM #8 3/8" Avery (Aggregates)	937 lb	2.780	5.40
ASTM C-33 Sand Avery (Aggregates)	2140 lb	2.722	12.60
ASTM C-494 Water Reducer (Admix)	24.44 floz (US)/yd³	1.125	0.03
Air	3.0 %.		0.82
Total :	4020		27.30